PURDUE UNIVERSITY
GRADUATE SCHOOL
Thesis/Dissertation Acceptance

This is to certify that the thesis/dissertation prepared

By Creasy Alexis Clauser

Entitled
IN VIVO TIBIAL LOADING OF HEALTHY AND OSTEOLATHRYTIC MICE

For the degree of   Master of Science in Biomedical Engineering

Is approved by the final examining committee:

Joseph Wallace
_____
Chair

Hiroki Yokota
_____

Jiliang Li
_____

To the best of my knowledge and as understood by the student in the Thesis/Dissertation Agreement, Publication Delay, and Certification Disclaimer (Graduate School Form 32), this thesis/dissertation adheres to the provisions of Purdue University's "Policy of Integrity in Research" and the use of copyright material.

Approved by Major Professor(s): Joseph Wallace

Approved by: Ken Yoshida   4/16/2015
_____
Head of the Departmental Graduate Program   Date

IN VIVO TIBIAL LOADING OF HEALTHY

AND OSTEOLATHRYTIC MICE

A Thesis

Submitted to the Faculty

of

Purdue University

by

Creasy A. Clauser

In Partial Fulfillment of the

Requirements for the Degree

of

Master of Science in Biomedical Engineering

May 2015

Purdue University

Indianapolis, Indiana

ACKNOWLEDGMENTS

Firstly, I cannot express enough my gratitude to my thesis advisor, Dr. Joseph Wallace, for providing the opportunity to work and grow professionally under his guidance. Without his insight and support this project would not have been possible. I would also like to thank him for always maintaining a focus on furthering the education of others and contributing to his field of work by holding high standards and emphasizing the importance of well-designed studies, as well as teaching courses that are relevant and up-to-date with current biomedical practices.

Secondly, I would like to thank the members of my advisory committee, Dr. Hiroki Yokota and Dr. Jiliang Li, for their input and guidance. In addition, I would like to thank Dr. Matt Allen and Dr. Keith Condon of the Indiana University Department of Anatomy and Cell Biology for their support and contributions to portions of my thesis project.

Thirdly, I would like to thank my research colleagues, Ms. Alycia Berman, Mr. Max Hammond, and Ms. Caitlin Wunderlin for their contributions and collaborative efforts to parts of this project, of which I could not have completed this work without.

Finally, I want to thank my parents, Allan and Brenda Clauser, and my grandmother, Janice Clauser, who have been my support system both when I am my best and worst self and taught by example that with hard work and dedication it is possible to both have a successful career and to put family first. Their support of my educational goals and encouragement to both pursue a career that I am passionate about and to become a well-rounded individual with integrity have enabled me to find success in the most difficult challenges that I have faced.

TABLE OF CONTENTS

LIST OF TABLES

LIST OF FIGURES

SYMBOLS

Symbol	Description, Unit
BFR/BS	bone formation rate, μm/day
BV/TV	bone volume fraction, %
CID	creep indentation distance, μm
Cr.Dn	crack density, $1/\text{mm}^2$
Cr.Le	crack length, μm
Cr.N	crack number
Cr.S.Dn	crack surface density, $\mu\text{m}/\text{mm}^2$
CSA	cross-sectional area, mm^2
ED	energy dissipation, μJ
ID	indentation distance, μm
IDI	indentation distance increase, μm
K	fracture stress intensity
MAR	mineral apposition rate, μm/day
MS/BS	mineralizing surface, %
SMI	structural model index
Tr.N	trabecular number, $1/\text{mm}^2$
Tr.S	trabecular spacing, μm
Tr.Th	trabecular thickness, μm
TID	total indentation distance, μm
TMD	tissue mineral density, g/cm^3
US	unloading slope, N/μm

ABBREVIATIONS

a	top loading span distance
BAPN	beta-aminopropionitrile
BS	bone surface
BS/TV	bone surface density
c	distance to neutral axis
CaHA	hydroxyapatite, pure crystal
CH_2	methylene
$CO_3{}^{2-}$	carbonate
dLS	double label
ECM	extracellular matrix
F	force
FWHM	full-width half maxima
I	moment of inertia
Ir.L.t	interlabel time
Ir.L.Th	interlabel width
L	bottom loading span distance
LOX	lysyl oxidase
MMR	mineral-to-matrix ratio
PBS	phosphate buffered saline
PMMA	polymethyl methacrylate
$PO_4{}^{3-}$	phosphate
RPI	reference point indentation
SEM	scanning electron microscopy
sLS	single label

μCT   micro computed tomography

vBMD   volumetric bone mineral density

ABSTRACT

Clauser, Creasy A. M.S.B.M.E., Purdue University, May 2015. In Vivo Tibial Loading of Healthy and Osteolathrytic Mice. Major Professor: Joseph M. Wallace.

Although the in vivo tibial loading model has been used to study the bone formation response of mice to exercise, little emphasis has been placed on the translation of architectural and compositional modifications to changes in mechanical behaviour. The goals of the studies discussed below were to investigate the mechanical response in both healthy and osteolathrytic mice to this loading model and to determine the dose-depended effects of strain level on these properties. In two separately designed studies, strain levels ranging from 1700 to 2400 $\mu\epsilon$ were applied to the right tibiae of 8 week old female C57BL/6 mice, while the left tibiae were used as non-loaded control. The first study consisted of loading both PBS- and BAPN-injected mice to 1750 $\mu\epsilon$ which resulted in little bone formation but some tissue-level changes in mechanical analyses and an improvement in fatigue-resistance in terms of microdamage accumulation. The second study loaded healthy mice to three strain levels (1700, 2050, and 2400 $\mu\epsilon$). Results indicated that the low end of the strain range did not engender a robust formation response, while the high end of the strain range resulted in a woven bone response in half of the animals in that group. Future studies will focus on the mid-strain level of 2050 $\mu\epsilon$ which induced both significant architectural and mechanical improvements.

1. INTRODUCTION

1.1   Bone Structure and Function

Bone is a dynamic hierarchical material that spans several orders of magnitude in length scale [1]. It has many functions, including structural support, housing of bone marrow, protection of vital organs, and mineral ion homeostasis, but the primary function is to support load and work in conjunction with muscles in order to make locomotion possible. In order to do so, bone must be mechanically strong under multidirectional forces and strains that come with a mobile lifestyle, a feat that is a function of geometry, mass, and material properties [2]. It is additionally important to understand that bone is not a static structure, but instead models as the skeleton matures and remodels in response to external stimuli.

Before describing the process of bone formation, it is necessary to describe the hierarchical structure of bone. Though there are many different bone types in the body, the primary focus of this thesis is on long bones, such as the tibia. The illustration below (Figure 1.1) demonstrates the different structures at each length scale within a long bone. On the whole bone level long bones are made up of cancellous (trabecular) bone in the proximal and distal ends, and cortical bone along the midshaft. Cortical bone is dense and provides a significant portion of a bones mechanical integrity. Trabecular bone is porous and composed of struts called trabeculae that vary in length and thickness and link together to create a three-dimensional network. This network is responsible for absorbing shock from loading and responding to deformation [4]. It is organized into lamellar sheets. Interestingly, both types of bone extracellular matrix (ECM) are composed primarily of collagen, the most abundant protein in the body [5]. Specifically, bone is made up of type I collagen, which comprises 90% of the total collagen content in the body [6]. The synthesis and organization of collagen in
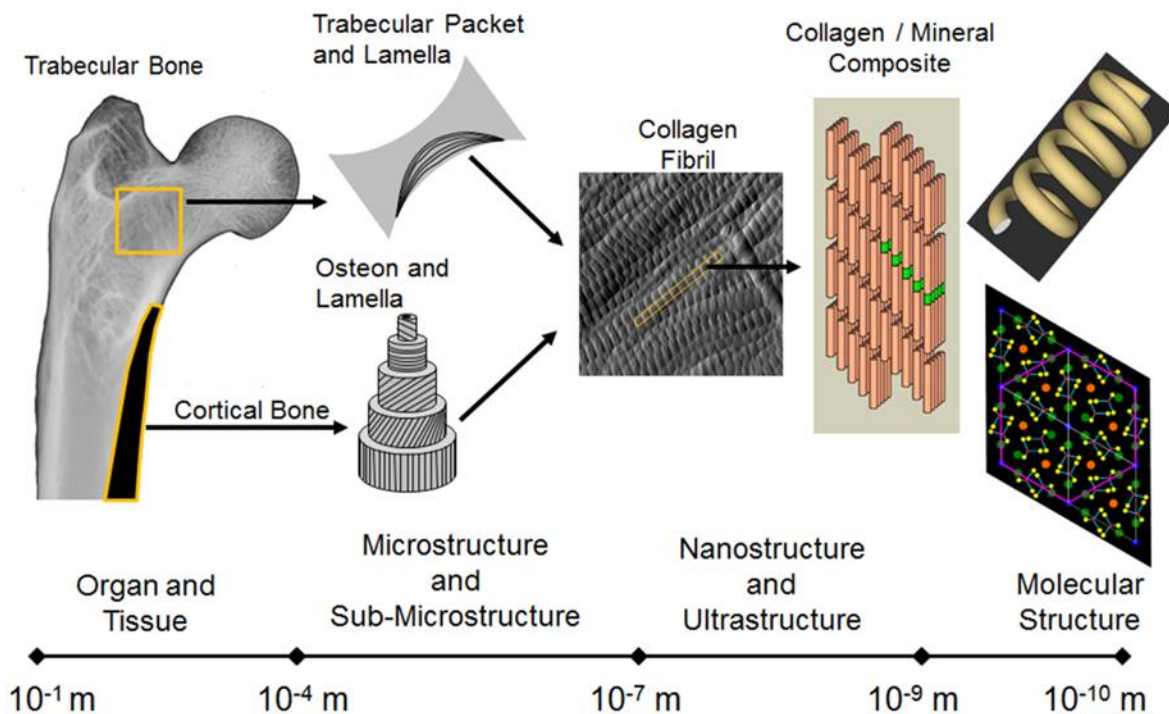
Fig. 1.1. Illustration of the hierarchical structure of bone from tissue level to molecular structure [3].

bone is discussed below. Additionally, mature bone has a mineral component which accounts for 2/3 of the weight of bone. This mineral is a form of geological hydroxyapatite [7]. The mineralization process occurs slowly as the crystals form and grow into fully mature crystalline lattices [8]. The organic and inorganic components of bone exist in different ratios depending on the main function and load environment of the particular bone. Bone has been shown to adapt both its chemical makeup and structural organization in response to mechanical stimulation, which will be discussed more in depth in subsequent sections.

1.2   Bone Growth and Remodeling

The skeleton grows and remodels over time, both in the radial and longitudinal directions. Remodeling involves removing old or damaged bone and replacing it with new bone. The skeleton is constantly remodeling. During early development, bone formation occurs faster than bone degradation. With age, the balance becomes constant, with formation and degradation being relatively equal. With old age, degradation can begin to overcome formation, resulting in bone deficiency diseases such as osteoporosis. The processes of bone growth and remodeling are a complex integration of three different types of cells: osteoclasts, osteoblasts, and osteocytes. Osteocytes reside in the bone extracellular matrix (ECM) and are sense and signaling cells. When bone is damaged, osteocytes sense the damage and signal to osteoclasts and osteoblasts to differentiate and migrate to the damaged area. The osteoclasts eat away the damaged bone, followed by osteoblasts that lay down new bone. In periods of bone growth, a complex process occurs, beginning with the generation of collagen.

Collagen synthesis begins on the cellular level in the endoplasmic reticulum. Three amino acid chains consisting of repeating triplets of glycine and other amino acid, represented by X and Y, are translated. Many prolines and some lysines in the X and Y positions are hydroxylated to provide chain stability. Next, glycosylation occurs. Disulfide bonds form between chains in the C-peptide region, providing the means for a molecular zipper to coil the three chains together into a right-handed triple helix [9]. The structure at this point is referred to as procollagen. The procollagen strands are transported from the endoplasmic reticulum to the Golgi apparatus and then out of the cell. During this process, peptidases cleave the C and N terminals. The now named tropocollagen strands assemble into fibrils. Multiple fibrils orient together to form the bone tissue. The newly formed tissue is then enzymatically cross-linked and mineralized over time, resulting in mature bone. The cross-linking process is important to the mechanics of bone [10, 11] and is discussed further at the end of this chapter.

1.3 Response to Mechanical Stimuli

As mentioned above, bone is a dynamic material. It has been shown that re-modelling of bone chemical makeup and structural organization occurs in response to external and internal stimuli [12–16]. The rates of bone response to load differ with age when comparing young, rapidly growing bone to mature, adult bone [17–19]. Using rodent models to investigate the mechanistic responses of bone to mechanical loading are useful in a lab setting. Exercise models such as running, jumping, and swimming have been used in mice and rats to induce bone adaptation [20–24]. These models are physiologically relevant but prevent having control over loading parameters, in addition to the whole-body systemic response both in the skeletal and other organ systems.

Alternatively, in vivo loading of the ulna has been successfully used in both mice and rats [25–27]. In addition the tibial loading model has been used over the last ten years to induce bone adaptation in mice [28, 29]. As with ulnar loading, this model provides control over experimental parameters such as load/strain magnitude, number of cycles, cyclic waveform, and frequency of loading which are uncontrollable or relatively controllable in exercise models. In addition, it allows for easier animal handling because the mice are maintained under anaesthesia for the duration of loading. In this loading model, direct compression loading is applied in the axial direction leading to a bending modality (Figure 1.2) which differs from the complex loading induced by running but allows for a more simplistic understanding of the load being applied. The advantage of tibial loading over ulnar loading is that the anatomy of the joints on either end of the tibia prevent direct loading on the surface of the tibia, instead transferring the load through the distal femur and calcaneus bone of the foot, compared to the ulnar model where load is applied directly to the olecranon process.

The tibial method of loading allows for experimental focus on the outcomes and mechanisms underlying a response to mechanical cues without having to consider systemic effects in the cardiovascular system. Because of these benefits, the model has
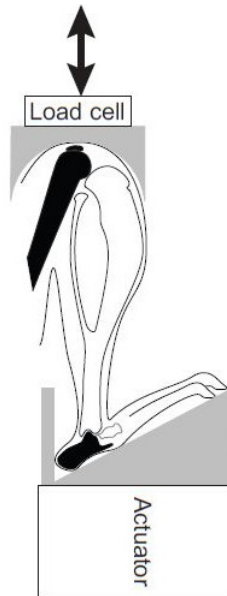
Fig. 1.2. Schematic of loading fixtures and direction of loading applied during in vivo tibial loading [30].

been used to determine the effects of loading on bone as a function of age [30–35], gender [36–38], inbred strain [39,40], disease [41,42], fracture healing [27], and load/strain level [28, 29, 43–46]. While many of these studies showed that loading significantly alters bone formation and structural architecture, few have looked at the effect of loading on mechanical properties. This is an important consideration that warrants investigation. Does increasing the quantity of bone improve bone structure and function in diseased models, or is it necessary to improve bone quality as well? In order to address this question, not only do structural properties need to be evaluated but also mechanical properties. Studies investigating load/strain level have consistently shown that higher magnitudes of load engender more a robust bone formation response, however it has been suggested that loading to even moderate levels can induce joint-damage and osteoarthritis [47,48]. As it has been shown that low levels of strain (800-1200 $\mu\epsilon$) will induce a detectable formation response [29,43], there may not be a

need to load to damaging strain levels to induce adequate bone formation to modify mechanical properties.

Although the tibial loading model has been frequently used over the past ten years, only three papers have addressed mechanical properties, including direct loading of a fracture site [49], axial loading to failure following 6 weeks of tibial loading [39], and an indirect calculation of elastic modulus using ash mineral density obtained from microcomputed tomography (μCT) [50]. Of these, the axial loading to failure study was most relevant to investigating mechanical properties affected by tibial loading. It was found that ultimate displacement, energy to failure, and ultimate force were significantly increased in loaded tibiae. However, in a pilot study performed to test proof of concept of the loading model, axial loading to failure by our methods resulted in frequent failure of the bone at the epiphysis. This could be due to the young age of mice being used in our studies, which are still rapidly growing and may not yet have fully fused growth plates.

1.4   Experimental Design

As noted above, bone mass, geometry, and material properties contribute to overall bone strength. Therefore, to fully investigate the effects of loading on bone strength, properties in all three categories should be assessed. One of the goals of this thesis was to evaluate each of these properties using a variety of outcomes.

First, to investigate geometric properties, the techniques of μCT and histomorphometry were used. μCT is a technique that uses a serial x-ray to create three-dimensional images of bone. These images can then be analyzed using post-processing tools. The usefulness of μCT in bone and mineral research has been described in the context of evaluating cortical and trabecular bone architecture [51]. Analysis of cortical bone allows for evaluation of geometric parameters such as cortical area, cortical thickness, total cross-sectional area, and tissue mineral density (TMD). Analysis of trabecular bone allows for evaluation of parameters such as bone volume frac-

tion (BV/TV), bone surface density (BS/TV), trabecular thickness (Tb.Th), number (Tb.N), spacing (Tb.S), connectivity, and structural model index (SMI) which is a measure of trabecular structure. An SMI close to 0 indicates plate-like struts, while a SMI close to 3 indicates struts like cylindrical rods. All of these parameters provide geometric and structural information about the bone.

Histomorphometry is a technique in which animals are injected in vivo with fluorescent markers. These markers are chelating agents that bind to calcium and are then incorporated into newly formed bone. After the bones are embedded and sectioned, the length and distance between markers injected a specific number of days apart (Ir.L.t) can be quantified in order to calculate mineralizing surface (MS/BS), mineral apposition rate (MAR) and bone formation rate (BFR/BS). MS/BS is the amount of periosteal or endocortical surface that has been mineralized normalized to the surface perimeter, indicative of osteoblast proliferation, number, and formation activity. MAR is the rate at which mineralization is occurring measured between two specific time points, indicative of the activity of individual teams of osteoblasts. BFR/BS combines the previous two parameters to evaluate the rate of bone formation normalized to the bone surface. Equations 1.1-1.3 below show the methods for calculating these parameters according to ASBMR standards [52]. The following measurements are obtained from the analysis and used in the equations below: bone perimeter, known as bone surface (BS), length of single (sLS) and double (dLS) calcein labels, and in the case of double labels the interlabel width (Ir.L.Th).

$$MS/BS = \frac{(\frac{1}{2}sLS + dLS)}{BS} * 100 \tag{1.1}$$

$$MAR = \frac{Ir.L.Th}{Ir.L.t} \tag{1.2}$$

$$BFR/BS = MS/BS * MAR \tag{1.3}$$

The mineral and organic chemical content of bone is also important to mechanical behavior. The relative content of organic and inorganic components in bone can be evaluated using Raman spectroscopy, a method that measures the vibrations of molecular bonds. For this technique, a laser is focused on the bone surface. The laser penetrates the bone surface, shifting the light energy through its interactions with the chemical bonds it encounters and is reflected back to a detector. The Raman shift is output in the form of a wavenumber diagram which is used to calculate the area under specific peaks (PO_4^{3-} (phosphate), CO_3^{2-} (carbonate), and various measures of collagen (amide III, CH_2 wag, and amide I envelope)). The full width at half maxima (FWHM) of the phosphate peak is measured and its inverse relates to crystallinity (the size, shape, and perfection of the mineral crystals). Matrix mineralization can be evaluated using the ratio of phosphate to collagen signals. Carbonate substitution is calculated using carbonate/phosphate. Amide I to amide III has been shown to provide insight to changes in secondary structure of collagen which is important because while amide III is relatively stable, amide I is very sensitive to polarization effects and collagen orientation. The use of this ratio helps to support matrix mineralization findings [53].

Finally, in order to relate tibial loading-induced bone growth to changes in mechanical properties, a question that has not been the focus of current literature, several mechanical testing methods can be applied. First, whole-bone mechanics can be assessed by using four-point bending to failure. From obtained load-displacement curves, stiffness, deformation characteristics (deformation to yield, postyield displacement, and total deformation), strength (yield force and ultimate force), and energy dissipation (work to yield, postyield work, and work to failure) can be calculated. Using geometry from μCT, force-displacement can be converted to stress-stain using the four-point bending equations shown below. From the new curves, elastic modulus, strain (strain to yield and strain to failure), stress (yield and ultimate), and toughness (preyield toughness (resilience) and total toughness) can be calculated.

$$\sigma = \frac{Fac}{2I} \tag{1.4}$$

$$\epsilon = \frac{6cd}{a(3L - 4a)} \tag{1.5}$$

The above equations (1.4 and 1.5) are functions of force (F), loading span distance (a), support loading span distance (L), distance from the fracture site to the neutral axis (c) obtained from μCT, and moment of inertia (I) about the bending axis obtained from μCT.

A second mechanical technique is fracture toughness. This technique involves creating an anatomically-sharp starter crack in the bone and then testing the bone to failure in three-point bending directly above this notch. Combined with scanning electron microscopy (SEM) images of the fracture surface, stable and unstable crack growth can be separated in order to calculate fracture toughness using a linear elastic fracture mechanics approach [54]. Testing of mouse femurs in a fracture toughness set-up was thoroughly described by Ritchie et al. [55] and adapted for use here in mouse tibiae.

Reference point indentation (RPI) allows for the determination of mechanical properties of the cortical diaphysis by cyclically-indenting the same location and evaluating properties such as material stiffness, creep, and energy dissipation. RPI is an advantageous testing method despite the damage caused to the bone surface because it can be used clinically to assess mechanical function and has been used to differentiate patient populations who are prone to fracture [56–59]. A schematic of the RPI method is shown in Figure 1.3.

It has been shown that the presence of microdamage in vivo triggers the initiation of intracortical bone remodelling [60], and that microdamage can be induced ex vivo by fatigue loading [61]. Microdamage can be induced by fatiguing bones to a stress level high enough to alter bone structure without catastrophically fracturing the bone. Subsequent en bloc fuchsin staining of the bones allows for the identification and
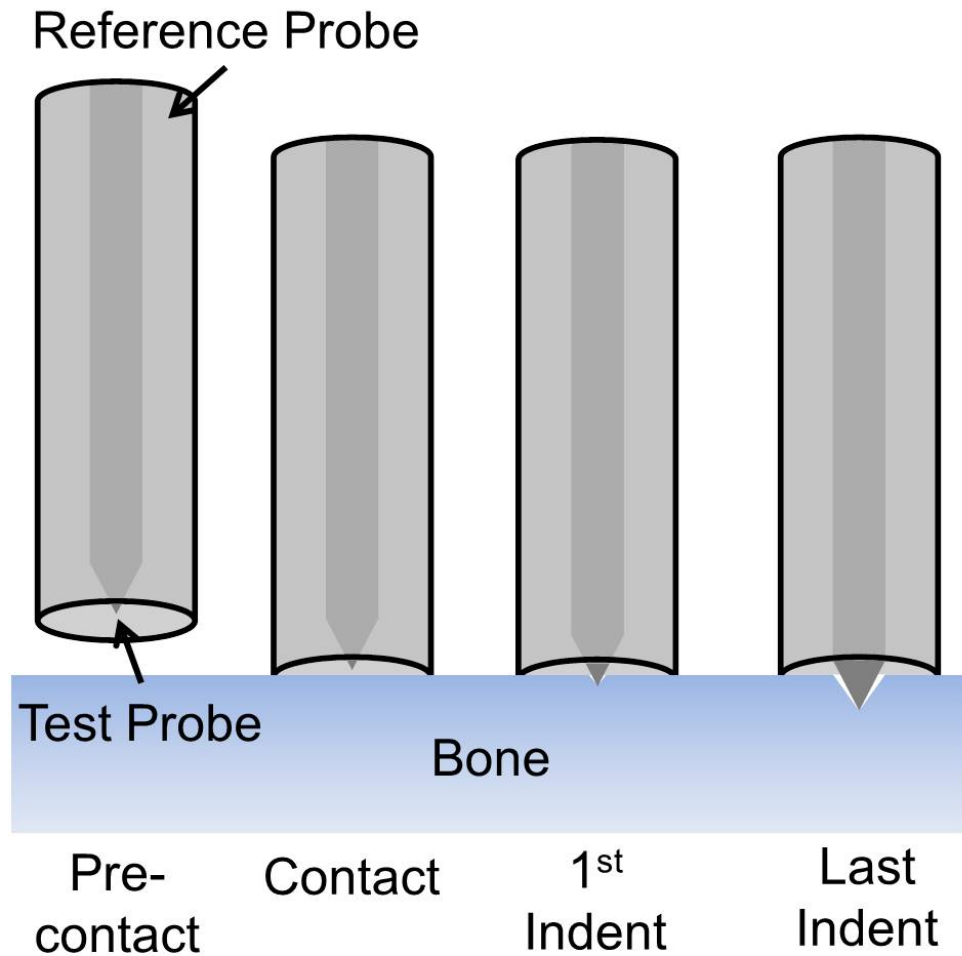
Fig. 1.3. A reference point indentation system includes a reference probe that is positioned on the bone surface and an indentation probe that repeatedly indents the bone. Figure courtesy of Max A. Hammond.

quantification of these cracks. The presence of microdamage in vivo has been linked to a decrease in bone toughness [62]. A goal of this study was to investigate if loading of bones in vivo changes the bone matrix in such a way as to protect them from ex vivo microdamage formation due to fatigue. Loading improves the quality of bone tissue, and this improvement may make it more resistive to damage that naturally occurs over time in vivo under normal loading and activity. Investigating damage produced via ex vivo fatigue will allow us to gain some insight into this possible mechanism.

If mechanical loading has the capacity to improve the mechanical properties of healthy bone, it is possible that it could be used as a therapeutic method to restore mechanical properties of diseased bone. In order to test this hypothesis, a disease model must be chosen. Osteolathrysm is a disease caused by over-ingestion of the seeds from the drought resistant lathyrus pea plant, which is commonly found in the areas of East Africa and Asia [63]. Consumed in excessive amounts, a compound inside of the seed called beta-aminopropionitrile (BAPN) induces a disruption in the collagen cross-linking process resulting in a cross-linking deficiency. BAPN reduces cross-linking by irreversibly binding to the lysyl oxidase (LOX) active site preventing the formation of telopeptide aldehydes and abolishing the formation of new cross-links (Figure 1.4) [64, 65]. This model can easily be induced in animals by injecting BAPN daily [66, 67]. Pre-existing bone is not affected while any newly formed bone is cross-link deficient. This is a simplistic and easily induced model of diseased bone with reduced mechanical properties.
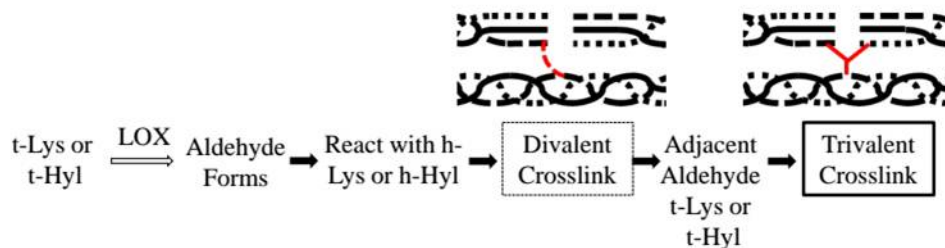
Fig. 1.4. Cross-linking pathway during collagen maturation process. BAPN irreversibly binds to LOX, which inhibits the formation of aldehydes necessary for cross-link formation. Figure courtesy of Max A. Hammond.

It should be noted that the concentration and volume of BAPN commonly injected in mice does not completely inhibit cross-link formation, but instead decreases the amount of cross-links formed. This partial inhibition in murine bone has been shown to cause a downward shift in collagen D-spacing and increased crystallinity [68].

1.5 References

[1] J.-Y. Rho, L. Kuhn-Spearing, and P. Zioupos, "Mechanical properties and the hierarchical structure of bone," *Medical Engineering and Physics*, vol. 20, no. 2, pp. 92–102, 1998.

[2] D. B. Burr, M. R. Forwood, D. P. Fyhrie, R. B. Martin, M. B. Schaffler, and C. H. Turner, "Bone microdamage and skeletal fragility in osteoporotic and stress fractures," *Journal of Bone and Mineral Research*, vol. 12, no. 1, pp. 6–15, 1997.

[3] D. B. Burr and O. Akkus, *Basic and Applied Bone Biology*, book section 4. Elsevier, 2014.

[4] J. K. Gong, J. S. Arnold, and S. H. Cohn, "Composition of trabecular and cortical bone," *The Anatomical Record*, vol. 149, no. 3, pp. 325–331, 1964.

[5] G. A. Di Lullo, S. M. Sweeney, J. Krkk, L. Ala-Kokko, and J. D. San Antonio, "Mapping the ligand-binding sites and disease-associated mutations on the most abundant protein in the human, type i collagen," *Journal of Biological Chemistry*, vol. 277, no. 6, pp. 4223–4231, 2002.

[6] D. J. Prockop and K. I. Kivirikko, "Collagens: molecular biology, diseases, and potentials for therapy," *Annu Rev Biochem*, vol. 64, pp. 403–34, 1995.

[7] A. S. Posner and G. Duyckaerts, "Infrared study of the carbonate in bone, teeth and francolite," *Experientia*, vol. 10, no. 10, pp. 424–5, 1954. Posner, a s Duyckaerts, g Journal Article Not Available Experientia. 1954 Oct 15;10(10):424-5.

[8] W. J. Landis, M. J. Song, A. Leith, L. McEwen, and B. F. McEwen, "Mineral and organic matrix interaction in normally calcifying tendon visualized in three dimensions by high-voltage electron microscopic tomography and graphic image reconstruction," *Journal of Structural Biology*, vol. 110, no. 1, pp. 39–54, 1993.

[9] A. Rich and F. H. C. Crick, "The molecular structure of collagen," *Journal of Molecular Biology*, vol. 3, no. 5, pp. 483–IN4, 1961.

[10] L. Knott and A. J. Bailey, "Collagen cross-links in mineralizing tissues: A review of their chemistry, function, and clinical relevance," *Bone*, vol. 22, no. 3, pp. 181–187, 1998.

[11] H. Oxlund, L. Sekilde, and G. rtoft, "Reduced concentration of collagen reducible cross links in human trabecular bone with respect to age and osteoporosis," *Bone*, vol. 19, no. 5, pp. 479–484, 1996.

[12] R. Chow, J. E. Harrison, and C. Notarius, *Effect of two randomised exercise programmes on bone mass of healthy postmenopausal women*, vol. 295. 1987.

[13] G. P. Dalsky, K. S. Stocke, A. A. Ehsani, E. Slatopolsky, W. C. Lee, and J. S. J. Birge, "Weight-bearing exercise training and lumbar bone mineral content in postmenopausal women," *Annals of Internal Medicine*, vol. 108, no. 6, pp. 824–828, 1988.

[14] D. P. Fyhrie, C. Milgrom, S. J. Hoshaw, A. Simkin, S. Dar, D. Drumb, and D. B. Burr, "Effect of fatiguing exercise on longitudinal bone strain as related to stress fracture in humans," *Annals of Biomedical Engineering*, vol. 26, no. 4, pp. 660–665, 1998.

[15] A. J. Kaneps, S. M. Stover, and N. E. Lane, "Changes in canine cortical and cancellous bone mechanical properties following immobilization and remobilization with exercise," *Bone*, vol. 21, no. 5, pp. 419–423, 1997.

[16] S. L. Woo, S. C. Kuei, D. Amiel, M. A. Gomez, W. C. Hayes, F. C. White, and W. H. Akeson, *The effect of prolonged physical training on the properties of long bone: a study of Wolff's Law*, vol. 63. 1981.

[17] K. Khan, H. A. McKay, H. Haapasalo, K. L. Bennell, M. R. Forwood, P. Kannus, and J. D. Wark, "Does childhood and adolescence provide a unique opportunity for exercise to strengthen the skeleton?," *Journal of Science and Medicine in Sport*, vol. 3, no. 2, pp. 150–164, 2000.

[18] A. Heinonen, H. Sievnen, P. Kannus, P. Oja, M. Pasanen, and I. Vuori, "High-impact exercise and bones of growing girls: A 9-month controlled trial," *Osteoporosis International*, vol. 11, no. 12, pp. 1010–1017, 2000.

[19] K. J. MacKelvie, K. M. Khan, M. A. Petit, P. A. Janssen, and H. A. McKay, "A school-based exercise intervention elicits substantial bone health benefits: A 2-year randomized controlled trial in girls," *Pediatrics*, vol. 112, no. 6, pp. e447–e452, 2003.

[20] P. Kannus, H. Sievnen, T. L. N. Jrvinen, M. Jrvinen, M. Kvist, P. Oja, I. Vuori, and L. Jozsa, "Effects of free mobilization and low- to high-intensity treadmill running on the immobilization-induced bone loss in rats," *Journal of Bone and Mineral Research*, vol. 9, no. 10, pp. 1613–1619, 1994.

[21] Y. Kodama, Y. Umemura, S. Nagasawa, W. G. Beamer, L. R. Donahue, C. R. Rosen, D. J. Baylink, and J. R. Farley, "Exercise and mechanical loading increase periosteal bone formation and whole bone strength in c57bl/6j mice but not in c3h/hej mice," *Calcified Tissue International*, vol. 66, no. 4, pp. 298–306, 2000.

[22] J. Mathey, M. N. Horcajada-Molteni, B. Chanteranne, C. Picherit, C. Puel, P. Lebecque, C. Cubizoles, M. J. Davicco, V. Coxam, and J. P. Barlet, "Bone mass in obese diabetic zucker rats: Influence of treadmill running," *Calcified Tissue International*, vol. 70, no. 4, pp. 305–311, 2002.

[23] A. Swissa-Sivan, A. Simkin, I. Leichter, A. Nyska, M. Nyska, M. Statter, A. Bivas, J. Menczel, and S. Samueloff, "Effect of swimming on bone growth and development in young rats," *Bone and Mineral*, vol. 7, no. 2, pp. 91–105, 1989.

[24] S. E. Warner, J. E. Shea, S. C. Miller, and J. M. Shaw, "Adaptations in cortical and trabecular bone in response to mechanical loading with and without weight bearing," *Calcified Tissue International*, vol. 79, no. 6, pp. 395–403, 2006.

[25] K. C. L. Lee, A. Maxwell, and L. E. Lanyon, "Validation of a technique for studying functional adaptation of the mouse ulna in response to mechanical loading," *Bone*, vol. 31, no. 3, pp. 407–412, 2002.

[26] K. Lee, H. Jessop, R. Suswillo, G. Zaman, and L. Lanyon, "The adaptive response of bone to mechanical loading in female transgenic mice is deficient in the absence of oestrogen receptor-alpha and -beta," *Journal of Endocrinology*, vol. 182, no. 2, pp. 193–201, 2004.

[27] M. D. Martinez, G. J. Schmid, J. A. McKenzie, D. M. Ornitz, and M. J. Silva, "Healing of non-displaced fractures produced by fatigue loading of the mouse ulna," *Bone*, vol. 46, no. 6, pp. 1604–12, 2010.

[28] R. L. De Souza, M. Matsuura, F. Eckstein, S. C. F. Rawlinson, L. E. Lanyon, and A. A. Pitsillides, "Non-invasive axial loading of mouse tibiae increases cortical bone formation and modifies trabecular organization: A new model to study cortical and cancellous compartments in a single loaded element," *Bone*, vol. 37, no. 6, pp. 810–818, 2005.

[29] J. C. Fritton, E. R. Myers, T. M. Wright, and M. C. van der Meulen, "Loading induces site-specific increases in mineral content assessed by microcomputed tomography of the mouse tibia," *Bone*, vol. 36, no. 6, pp. 1030–8, 2005.

[30] R. P. Main, M. E. Lynch, and M. C. van der Meulen, "Load-induced changes in bone stiffness and cancellous and cortical bone mass following tibial compression diminish with age in female mice," *J Exp Biol*, vol. 217, no. Pt 10, pp. 1775–83, 2014.

[31] N. Holguin, M. D. Brodt, M. E. Sanchez, and M. J. Silva, "Aging diminishes lamellar and woven bone formation induced by tibial compression in adult c57bl/6," *Bone*, vol. 65, pp. 83–91, 2014.

[32] T. K. Patel, M. D. Brodt, and M. J. Silva, "Experimental and finite element analysis of strains induced by axial tibial compression in young-adult and old female c57bl/6 mice," *J Biomech*, vol. 47, no. 2, pp. 451–7, 2014.

[33] M. J. Silva, M. D. Brodt, M. A. Lynch, A. L. Stephens, D. J. Wood, and R. Civitelli, "Tibial loading increases osteogenic gene expression and cortical bone volume in mature and middle-aged mice," *PLoS ONE*, vol. 7, no. 4, p. e34980, 2012.

[34] M. D. Brodt and M. J. Silva, "Aged mice have enhanced endocortical response and normal periosteal response compared with young-adult mice following 1 week of axial tibial compression," *J Bone Miner Res*, vol. 25, no. 9, pp. 2006–15, 2010.

[35] R. P. Main, M. E. Lynch, and M. C. H. van der Meulen, "In vivo tibial stiffness is maintained by whole bone morphology and cross-sectional geometry in growing female mice," *Journal of Biomechanics*, vol. 43, no. 14, pp. 2689–2694, 2010.

[36] M. E. Lynch, R. P. Main, Q. Xu, D. J. Walsh, M. B. Schaffler, T. M. Wright, and M. C. van der Meulen, "Cancellous bone adaptation to tibial compression is not sex dependent in growing mice," *J Appl Physiol (1985)*, vol. 109, no. 3, pp. 685–91, 2010.

[37] L. B. Meakin, T. Sugiyama, G. L. Galea, W. J. Browne, L. E. Lanyon, and J. S. Price, "Male mice housed in groups engage in frequent fighting and show a lower response to additional bone loading than females or individually housed males that do not fight," *Bone*, vol. 54, no. 1, pp. 113–7, 2013.

[38] L. B. Meakin, G. L. Galea, T. Sugiyama, L. E. Lanyon, and J. S. Price, "Age-related impairment of bones' adaptive response to loading in mice is associated with sex-related deficiencies in osteoblasts but no change in osteocytes," *J Bone Miner Res*, vol. 29, no. 8, pp. 1859–71, 2014.

[39] N. Holguin, M. D. Brodt, M. E. Sanchez, A. A. Kotiya, and M. J. Silva, "Adaptation of tibial structure and strength to axial compression depends on loading history in both c57bl/6 and balb/c mice," *Calcif Tissue Int*, vol. 93, no. 3, pp. 211–21, 2013.

[40] A. Morse, M. M. McDonald, N. H. Kelly, K. M. Melville, A. Schindeler, I. Kramer, M. Kneissel, M. C. van der Meulen, and D. G. Little, "Mechanical load increases in bone formation via a sclerostin-independent pathway," *J Bone Miner Res*, vol. 29, no. 11, pp. 2456–67, 2014.

[41] M. E. Lynch, D. Brooks, S. Mohanan, M. J. Lee, P. Polamraju, K. Dent, L. J. Bonassar, M. C. van der Meulen, and C. Fischbach, "In vivo tibial compression decreases osteolysis and tumor formation in a human metastatic breast cancer model," *J Bone Miner Res*, vol. 28, no. 11, pp. 2357–67, 2013.

[42] C. Ciani, D. Sharma, S. B. Doty, and S. P. Fritton, "Ovariectomy enhances mechanical load-induced solute transport around osteocytes in rat cancellous bone," *Bone*, vol. 59, no. 0, pp. 229–234, 2014.

[43] M. E. Lynch, R. P. Main, Q. Xu, T. L. Schmicker, M. B. Schaffler, T. M. Wright, and M. C. van der Meulen, "Tibial compression is anabolic in the adult mouse skeleton despite reduced responsiveness with aging," *Bone*, vol. 49, no. 3, pp. 439–46, 2011.

[44] T. Sugiyama, L. B. Meakin, W. J. Browne, G. L. Galea, J. S. Price, and L. E. Lanyon, "Bones' adaptive response to mechanical loading is essentially linear between the low strains associated with disuse and the high strains associated with the lamellar/woven bone transition," *J Bone Miner Res*, vol. 27, no. 8, pp. 1784–93, 2012.

[45] A. M. Weatherholt, R. K. Fuchs, and S. J. Warden, "Cortical and trabecular bone adaptation to incremental load magnitudes using the mouse tibial axial compression loading model," *Bone*, vol. 52, no. 1, pp. 372–379, 2013.

[46] J. Nguyen, S. Y. Tang, D. Nguyen, and T. Alliston, "Load regulates bone formation and sclerostin expression through a tgfbeta-dependent mechanism," *PLoS One*, vol. 8, no. 1, p. e53813, 2013.

[47] E. L. Radin, R. B. Martin, D. B. Burr, B. Caterson, R. D. Boyd, and C. Goodwin, "Effects of mechanical loading on the tissues of the rabbit knee," *Journal of Orthopaedic Research*, vol. 2, no. 3, pp. 221–234, 1984.

[48] F. C. Ko, C. Dragomir, D. A. Plumb, S. R. Goldring, T. M. Wright, M. B. Goldring, and M. C. van der Meulen, "In vivo cyclic compression causes cartilage degeneration and subchondral bone changes in mouse tibiae," *Arthritis Rheum*, vol. 65, no. 6, pp. 1569–78, 2013.

[49] M. J. Gardner, M. C. H. v. d. Meulen, D. Demetrakopoulos, T. M. Wright, E. R. Myers, and M. P. Bostrom, "In vivo cyclic axial compression affects bone healing in the mouse tibia," *Journal of orthopaedic research : official publication of the Orthopaedic Research Society*, vol. 24, no. 8, pp. 1679–1686, 2006.

[50] H. Razi, A. I. Birkhold, P. Zaslansky, R. Weinkamer, G. N. Duda, B. M. Willie, and S. Checa, "Skeletal maturity leads to a reduction in the strain magnitudes induced within the bone: A murine tibia study," *Acta Biomaterialia*, vol. 13, no. 0, pp. 301–310, 2015.

[51] Z. Bart and J. Wallace, "Microcomputed tomography applications in bone and mineral research," *ACT*, vol. 2, no. 3, pp. 121–127, 2013.

[52] D. W. Dempster, J. E. Compston, M. K. Drezner, F. H. Glorieux, J. A. Kanis, H. Malluche, P. J. Meunier, S. M. Ott, R. R. Recker, and A. M. Parfitt, "Standardized nomenclature, symbols, and units for bone histomorphometry: A 2012 update of the report of the asbmr histomorphometry nomenclature committee," *Journal of Bone and Mineral Research*, vol. 28, no. 1, pp. 2–17, 2013.

[53] Z. R. Bart, M. A. Hammond, and J. M. Wallace, "Multi-scale analysis of bone chemistry, morphology and mechanics in the oim model of osteogenesis imperfecta," *Connective Tissue Research*, vol. 55, no. S1, pp. 4–8, 2014.

[54] A. E399-09, "Standard test method for linear-elastic plane-strain fracture toughness, k ic of metallic materials," *ASTM International*, 2009.

[55] R. O. Ritchie, K. J. Koester, S. Ionova, W. Yao, N. E. Lane, and J. W. Ager, "Measurement of the toughness of bone: A tutorial with special reference to small animal studies()," *Bone*, vol. 43, no. 5, pp. 798–812, 2008.

[56] M. A. Gallant, D. M. Brown, J. M. Organ, M. R. Allen, and D. B. Burr, "Reference-point indentation correlates with bone toughness assessed using whole-bone traditional mechanical testing," *Bone*, vol. 53, no. 1, pp. 301–305, 2012.

[57] D. Bridges, C. Randall, and P. K. Hansma, "A new device for performing reference point indentation without a reference probe," *Review of Scientific Instruments*, vol. 83, no. 4, p. 044301, 2012.

[58] C. Randall, D. Bridges, R. Guerri, X. Nogues, L. Puig, E. Torres, L. Mellibovsky, K. Hoffseth, T. Stalbaum, A. Srikanth, J. C. Weaver, S. Rosen, H. Barnard, D. Brimer, A. Proctor, J. Candy, C. Saldana, S. Chandrasekar, T. Lescun, C. M. Nielson, E. Orwoll, D. Herthel, H. Kopeikin, H. T. Y. Yang, J. N. Farr, L. McCready, S. Khosla, A. Diez-Perez, and P. K. Hansma, "Applications of a new handheld reference point indentation instrument measuring bone material strength," *Journal of Medical Devices*, vol. 7, no. 4, pp. 0410051–0410056, 2013.

[59] A. Diez-Perez, R. Gerri, X. Nogues, E. Cceres, M. J. Pea, L. Mellibovsky, C. Randall, D. Bridges, J. C. Weaver, A. Proctor, D. Brimer, K. J. Koester, R. O. Ritchie, and P. K. Hansma, "Microindentation for in vivo measurement of bone tissue mechanical properties in humans," *Journal of Bone and Mineral Research*, vol. 25, no. 8, pp. 1877–1885, 2010.

[60] D. B. Burr, R. B. Martin, M. B. Schaffler, and E. L. Radin, "Bone remodeling in response to in vivo fatigue microdamage," *Journal of Biomechanics*, vol. 18, no. 3, pp. 189–200, 1985.

[61] R. B. Martin, "Fatigue microdamage as an essential element of bone mechanics and biology," *Calcified Tissue International*, vol. 73, no. 2, pp. 101–107, 2003.

[62] P. Zioupos, "Accumulation of in-vivo fatigue microdamage and its relation to biomechanical properties in ageing human cortical bone," *Journal of Microscopy*, vol. 201, no. 2, pp. 270–278, 2001.

[63] B. J. Geiger, H. Steenbock, and H. T. Parsons, "Lathyrism in the rat," *Nutrition Reviews*, vol. 34, no. 8, pp. 240–241, 1976.

[64] R. C. Siegel, S. R. Pinnell, and G. R. Martin, "Cross-linking of collagen and elastin. properties of lysyl oxidase," *Biochemistry*, vol. 9, no. 23, pp. 4486–92, 1970.

[65] M. Yamauchi and M. Sricholpech, "Lysine post-translational modifications of collagen," *Essays Biochem*, vol. 52, pp. 113–33, 2012.

[66] C. Machon, B. Le Calve, S. Coste, M. Riviere, L. Payen, D. Bernard, and J. Guitton, "Quantification of beta-aminopropionitrile, an inhibitor of lysyl oxidase activity, in plasma and tumor of mice by liquid chromatography tandem mass spectrometry," *Biomed Chromatogr*, vol. 28, no. 7, pp. 1017–23, 2014.

[67] M. B. Sevil, M. J. Anadon-Baselga, M. T. Frejo, E. Llama, and M. A. Capo, "Pharmacokinetic analysis of beta-aminopropionitrile in rabbits," *Vet Res*, vol. 27, no. 2, pp. 117–23, 1996.

[68] M. Hammond and J. Wallace, "Exercise prevents -aminopropionitrile-induced morphological changes to type i collagen in murine bone.," *BoneKEy Reports*, vol. 4, 2015.

2. LOW STRAIN TIBIAL LOADING STUDY

Based on the understanding of the in vivo tibial loading model and effect of mechanical loading on mice, along with the investigative techniques discussed in the introduction, the following hypotheses and experimental design were made. It was hypothesized that loading of mice to a relatively low strain level would improve mechanical properties, that loading can prevent the degradation of properties in a drug-induced disease model, and that loading will better equip bones to resist the formation of ex vivo fatigue-induced damage.

2.1 Materials and Methods

2.1.1 Animals

Animals (n = 109, female, C57BL/6NHsd) were obtained from Harlan Laboratories at approximately 7 weeks of age and allowed to acclimate for one week prior to the start of in vivo loading. Animals were handled following Indiana University School of Science Institutional Animal Care and Use Committee (IACUC) approval (SC210R) and group-housed with access to food, water and cage activity ad libitum in a light/dark controlled room. Body weight was recorded one day prior to the beginning of loading and animals were randomly sorted into weight-matched groups (n = 5 calibration, n = 52 PBS, n = 52 BAPN). Animals were weighed every other day after the start of loading to assess overall health. From 8 weeks of age until sacrifice, animals in the disease group were subcutaneously injected daily with 0.2 mL of BAPN (300 mg/kg) in solution with sterile phosphate buffered saline (PBS), and animals in the control group were injected daily with 0.2 mL of sterile PBS. Animals were sacrificed at 10 weeks of age via CO_2 inhalation. In addition to the PBS or

BAPN injection, 40 mice (20 control, 20 BAPN) were given intraperitoneal injections of calcein (30 mg/kg of 0.6% calcein) on days three and ten to quantify the dynamics of new bone formation.

2.1.2   Load-Strain Calibration

One day prior to beginning in vivo loading, five mice were sacrificed via CO_2 inhalation. Immediately after sacrifice, a small incision was made through the skin of the right tibia of each mouse in order to attach a single-element microstrain gauge (Vishay, Shelton, CT: EA-06-015DJ-120) to the anteromedial surface of the bone, proximal to the tibia-fibula junction [1]. The exposed bone surface was first cleaned using chloroform and the gauge was attached using an adhesive kit (M-Bond 200). After drying, the gauge was coated with polyurethane (M-Coat A). Using a mechanical testing machine (Bose Corporation, Eden Prarie, MN: Electroforce 3200) and a custom loading fixture, the tibiae were loaded using a 2 Hz sine wave and load was stepped up from 2 N to 12 N in 1 N increments. Load and strain were recorded simultaneously. Load vs. strain curves were plotted and a linear fit was applied to obtain the relationship between load and strain. Using this calibration curve, it was determined that to achieve 1750 $\mu\epsilon$ an applied compressive load of -7 N needs to be applied.

2.1.3   In Vivo Loading

The right tibiae of all PBS and BAPN injected mice (n = 52 per group) were loaded in vivo. Isoflurane-induced anaesthesia (2%) was used to anesthetize mice prior to loading and mice were maintained under anesthesia for the duration of loading. The right tibiae were loaded (cyclic compression, 2 Hz) over a 14 day period with a day of rest after every third day of loading, resulting in 9 loading days (Figure 2.1). The loading profile consisted of four haversine waveforms followed by 3 seconds of rest repeated 55 times for a total of 220 cycles of loading per day. After the final

bout of loading, mice were allowed to rest for two days before sacrifice. Animals were euthanized at 10 weeks of age via CO_2 inhalation. Right and left tibiae were harvested, total length was measured using calipers, and each bone was wrapped in PBS-soaked gauze and stored at -20 °C.

Day	Event
-1	Weigh and group
0	Calibration
1-3	Load
4	Rest
5-7	Load
8	Rest
9-11	Load
12-13	Rest
14	Sacrifice
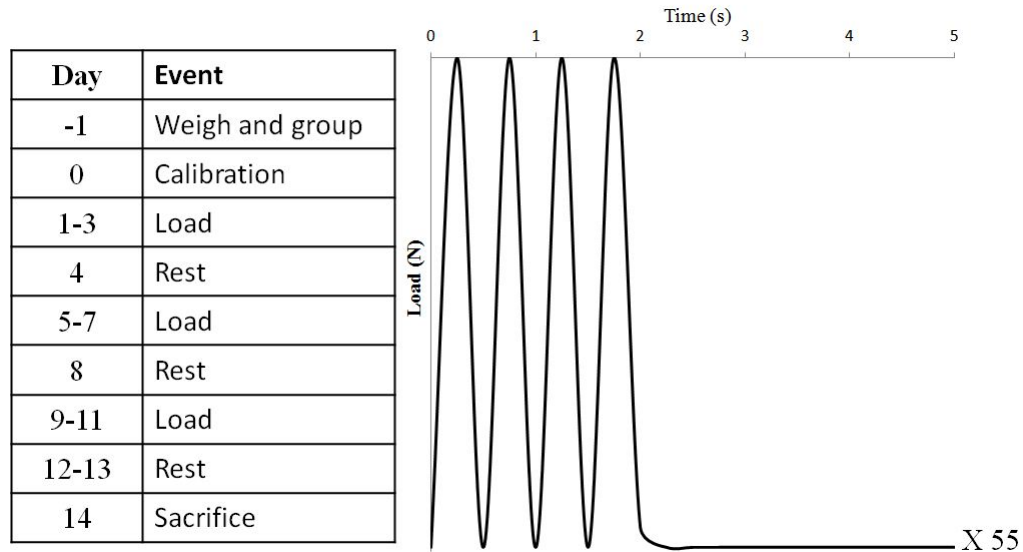
Fig. 2.1. Schematic of loading schedule and profile used in tibial loading experiment.

2.1.4 Microcomputed Tomography

88 full tibiae (n = 22 per group) were scanned using a high-resolution μCT system, (Bruker-MicroCT, Kontich, Belgium: Skyscan 1172) in order to obtain geometric measurements. Calibration was performed daily prior to scanning the bones using two cylindrical hydroxyapatite phantoms (0.25 and 0.75 g/cm^3 CaHA). Scans were performed at an isotropic voxel size of 17.2 μm resolution (V = 50 kV, I = 167 μA). Scans were reconstructed for use in cortical and trabecular analyses.

For cortical bone analysis,a standard diaphyseal site was chosen to be 1.5 mm proximal to the tibia-fibula junction. Seven transverse slices were obtained from this site and converted to binary images using a standard greyscale threshold value of 60.

Geometric properties and tissue mineral density (TMD) were obtained from these images.

Trabecular analysis was performed on 12% of the total length of the bone in the proximal metaphysis, starting at the distal end of the growth plate and extending distally. Regions of interest including only trabecular bone were automatically segmented using a custom Matlab code. Parameters of trabecular architecture and volumetric bone mineral density (vBMD) were obtained.

2.1.5   Four-Point Bending to Failure

Following μCT, 44 tibiae (n = 11 per group) were monotonically tested to failure using four-point bending in displacement control at 0.025 mm/sec while fully hydrated. A loading span of 3 mm and support span of 9 mm were used. The tibia-fibula junction was placed just outside of the right-most loading point and oriented such that the bone was tested in the medial-lateral direction with the medial surface in tension. The distance from the distal end of the bone to the location of fracture initiation was measured using calipers. Seven transverse slices were obtained from the μCT images at the location of fracture and calculated geometric properties (bending moment of inertia and distance from the centroid to the extreme fiber in tension) were used to map load-displacement to stress-strain. Pre- and post-yield mechanical properties were obtained from the resulting curves, as previously described [2].

2.1.6   Fracture Toughness

44 tibiae (n = 11 per group) were hand-notched with a scalpel blade in an alumina suspension such that the notch entered the intramedullary cavity but did not proceed more than halfway through the bone. The location of the notch was in the anterior-medial region of the mid-diaphysis, proximal to the tibia-fibula junction. After notching, bones were tested in three-point bending with the notched side in tension and the notch located directly under the applied load. The tibiae were tested

to failure at 0.001 mm/sec. After the test, the distance to the fracture site was measured using calipers, which was then used in conjunction with μCT to determine the structural properties at the location of fracture. Following the mechanical testing, bones were dehydrated with graded ethanol, mounted, gold-coated, and then the fracture surface was imaged using SEM. Images obtained were used to determine the angles of stable and unstable crack growth. The force and displacement data from the mechanical test, the structural properties from the μCT, and the crack growth angles from the SEM were then used in a custom MATLAB script to determine fracture stress intensity (K) as described by Ritchie et al. [3].

2.1.7 Raman Spectroscopy
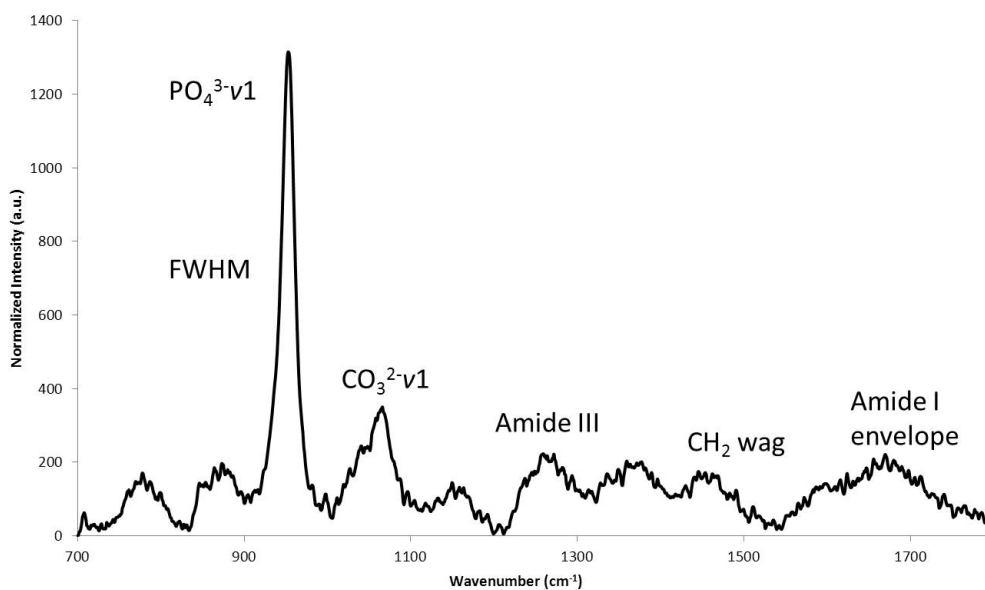
Fig. 2.2. A representative Raman spectrum with baseline-corrected and labeled peaks of interest. Ratios of interest were PO_4^{3-}/Amide I, PO_4^{3-}/CH$_2$ wag, PO_4^{3-}/Amide III, CO_3^{2-}/PO_4^{3-}, and Amide I/Amide III. Crystallinity is calculated using 1/FWHM.

Raman spectroscopy was performed using a LabRAM HR 800 Raman Spectrometer (HORIBA Jobin Yvon, Edison, NJ) paired with a BX41 microscope (Olympus, Tokyo, Japan), as previously described [4]. The posterior surface of 40 whole tibiae (n = 10 per group) was gently scraped using a flat scalpel blade to remove the periosteum. The bone was then placed in a petri dish modified with a foam support to orient the bone with the posterior surface facing upwards. The dish was filled with enough PBS to saturate the foam but not submerge the bone. The dish was then placed under the microscope, and a 50X objective was used to focus a spot size of approximately 10 μm on the surface. Three to five locations approximately 1mm apart and distal to the tibia-fibula junction were acquired for each sample. Five 20 second acquisitions were averaged into a single spectrum at each location and baseline corrected (LabSpec 5, HORIBA Jobin Yvon). OriginPro 8.6 (OriginLab, Northampton, MA) was used to fit a single Guassian peak to the PO_4^{3-} peak. Additional peaks (CO_3^{2-}, Amide III, CH_2 wag, and Amide I envelope) were located and the area under each peak was calculated at each axial location. The locations were then pooled into a single value from each bone. Ratios of these peak areas have been shown to correlate to various compositional parameters. The full width at half maxima (FWHM) of the phosphate peak was measured and its inverse relates to crystallinity. Matrix mineralization (MMR) was calculated using three ratios, phosphate/amide I (MMR Amide I), phosphate/CH_2 wag (MMR CH_2), and phosphate/amide III (MMR Amide III). Carbonate substitution is calculated using carbonate/phosphate. Amide I/amide III has been shown to provide insight to the changes in secondary structure [5]. A representative baseline-fit Raman spectrum is shown in Figure 2.2.

2.1.8   Reference Point Indentation

The same 40 tibia used for Raman spectroscopy were tested using a Biodent Reference Point Indentation (RPI) system (Active Life Scientific, Santa Barbara, CA). Calibration indents were first performed on a PMMA block. Bones were submerged up

to but not covering the indentation surface in PBS. The posterior surface of each bone was cyclically indented (10 cycles, 2 N, 2 Hz) at 4 locations approximately 1 mm apart and distal to the tibia-fibula junction in regions that roughly corresponded to those used for Raman. A custom MATLAB program was used to analyze each indentation cycle to calculate indentation distance (ID), energy dissipation (ED), unloading slope (US), and creep indentation distance (CID) of the first cycle and indentation distance increase (IDI) , total indentation distance (TID), total energy dissipation, average CID, average ED, and average US of each remaining cycle (2-10). The locations of measure of some of these parameters are indicated in the schematic of an RPI force-distance output curve in Figure 2.3. If the initial indentation distance was determined to be much greater than the group average, it was excluded. Therefore 3-4 indentation locations were averaged to create a single value per parameter measured for each bone.
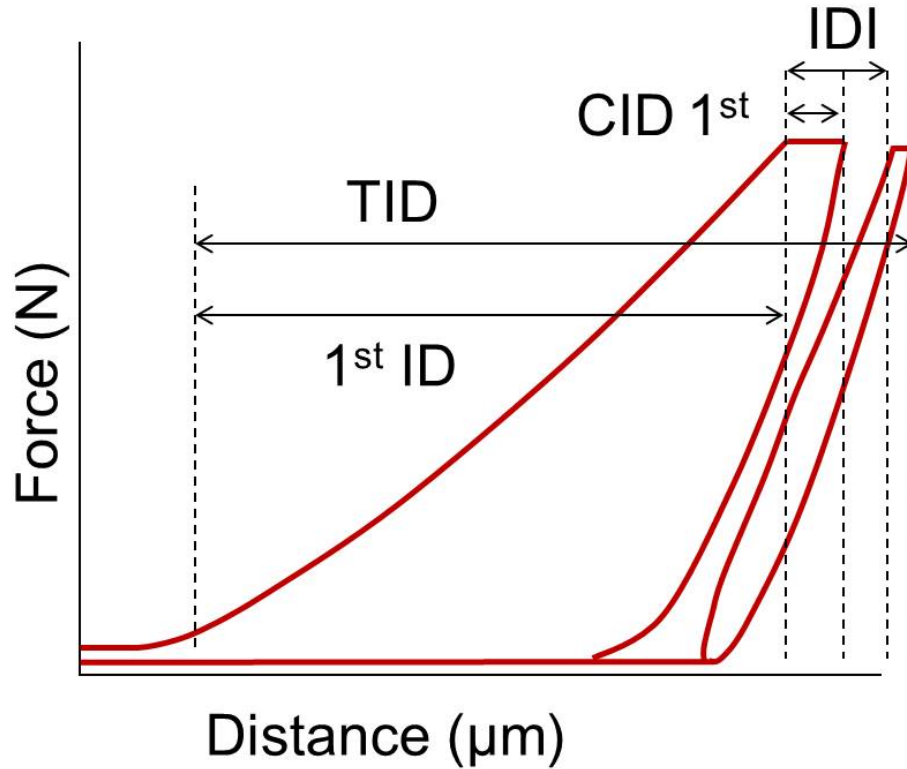
Fig. 2.3. Schematic of RPI cyclic indentation and measured parameters. Figure courtesy of Max A. Hammond.

2.1.9 Ex Vivo Fatigue

Using the cortical geometric and mechanical analysis data, the average force required to achieve 120 MPa in 4-point bending was found to be 8.2 N. This value is 67% of the ultimate stress from the non-loaded control group subjected to four-point bending to failure. 40 tibiae (n = 10 per group) from mice that received calcein injections were loaded in four-point bending in fatigue (20,000 cycles, 2 Hz, haversine) to this force using a mechanical testing machine. Bones were kept hydrated by fully submerging in lactate Ringers solution for the duration of the fatigue profile. Before and after fatigue, a single load-unload curve (0.5 Hz, haversine, 8 N) was taken to evaluate the change in stiffness and energy dissipation due to fatigue.

2.1.10 Dynamic Histomorphometry and Microdamage Analysis

The 40 fatigued bones (n = 10 per group) and 40 non-fatigued bones (n = 10 per group), all from the 40 animals that received calcein injections, were dehydrated, stained en bloc with basic fuchsin, and embedded in polymethyl methacrylate (PMMA). Six 120 μm-thick sections proximal to the tibia-fibula junction were obtained using a diamond-wire saw. Two sections were cleaned and fixed to slides to be examined for microdamage analysis. Two different sections were hand ground to approximately 40 μm using 600 then 400 grit sand paper, then cleaned and fixed to slides for histomorphometric analysis. The remaining two sections were kept in case of damaged or unmeasurable sections, but otherwise not measured.

Histomorphometric analysis was performed (n = 2 slides per bone analysed) using a fluorescence microscope system (Nikon Optihot-2, X-cite 120 UV System) and Bio-Quant software (Bioquant Osteo 2012) to measure bone perimeter (BS), area, length of single (sLS) and double (dLS) calcein labels, and in the case of double labels the interlabel thickness (Ir.L.Th) to assess mineralizing surface (MS/BS), mineral apposition rate (MAR), and bone formation rate (BFR) on both the endocortical and periosteal surfaces. In the event that no labels were present on either surface, the values from those bones were excluded from analysis. If no Ir.L.Th was measurable on a surface, the values for MAR and BFR were excluded from analysis.

Length measurements were pooled from the two analysed slides per bone into a single value for each measure. Microdamage analysis was performed on the same system (n = 2 slides per bone analysed). Cracks were measured to obtain number of cracks (Cr.N), average crack length (Cr.Le), crack density (Cr.Dn), and crack surface density (Cr.S.Dn). All measurements were pooled into a single value for each bone. Analyses were performed first including all samples, and then again excluding bones with no cracks present.

2.1.11 Statistics

All values are reported as mean $\pm$ standard deviation. All data sets were checked for normality and homogeneity and any violations were restored using transformations. For all comparisons except fatigue analysis, 2-way ANOVA with main effects of loading and disease were performed with $p < 0.05$ being significant. For cases of interactions between main effects, a one-way ANOVA was performed and if significant ($p < 0.05$) a Tukeys HSD post hoc test was performed to compare groups ($p < 0.05$). For the fatigue analysis, repeated-measures ANOVA with main effects of fatigue, loading, and disease were performed with $p < 0.05$ being significant. Statistical tests were performed using SAS 9.4 (SAS Institute Inc., Cary, NC).

2.1.12 Methods Overview

Below is a schematic overview of the methods and group sample sizes used in this study. Study outcomes are shaded in gray. Calibration mice are not included. It should be noted that the shown sample sizes are the intended sample size per group for each method, not the sample sizes used in the analysis. A detailed explanation of the sample sizes used for each method in the analysis can be found in the results section below.
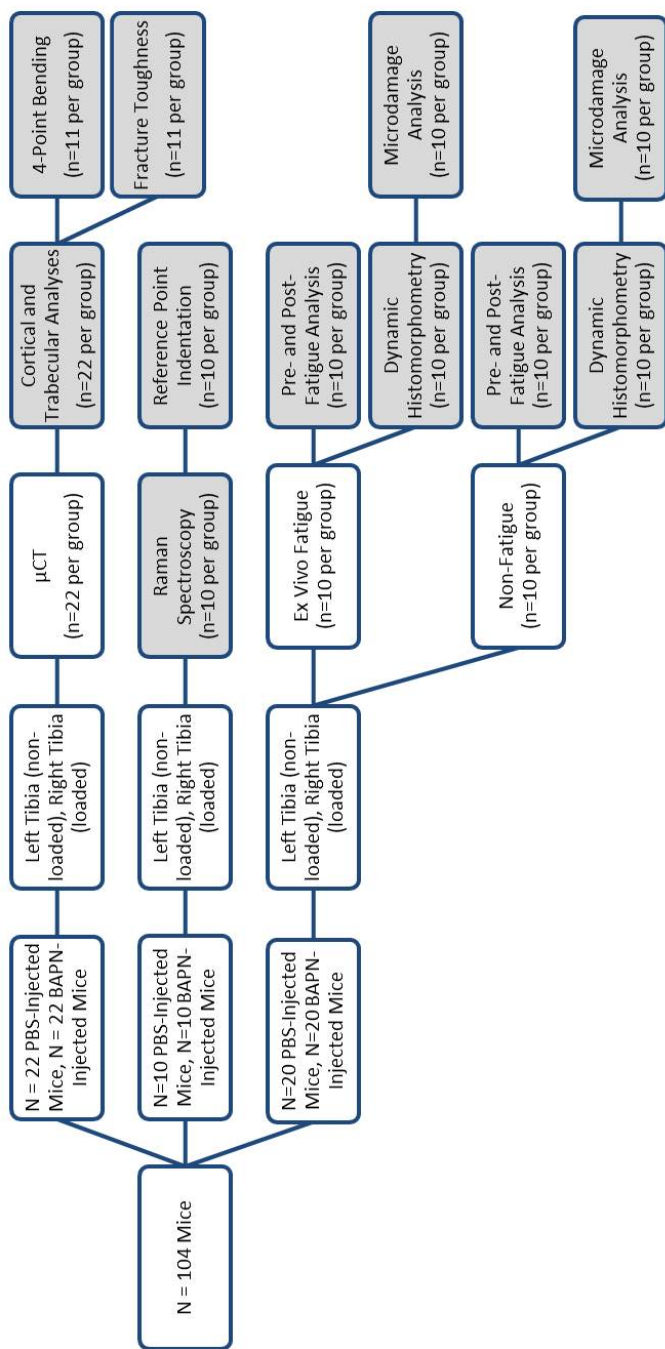
Fig. 2.4. Schematic overview of low strain tibial loading study outcomes including initial sample sizes.

2.2   Results

2.2.1   Calibration

Strain calibration was successfully performed. The linear-fit calibration curve is shown in Fig. 2.5 below. Data points from 12 N were excluded due to observable changes in bending at that load level which could have been a result of the load level itself but is more likely due to the progressive increase in load combined with the stiffening of the surrounding tissues with time.
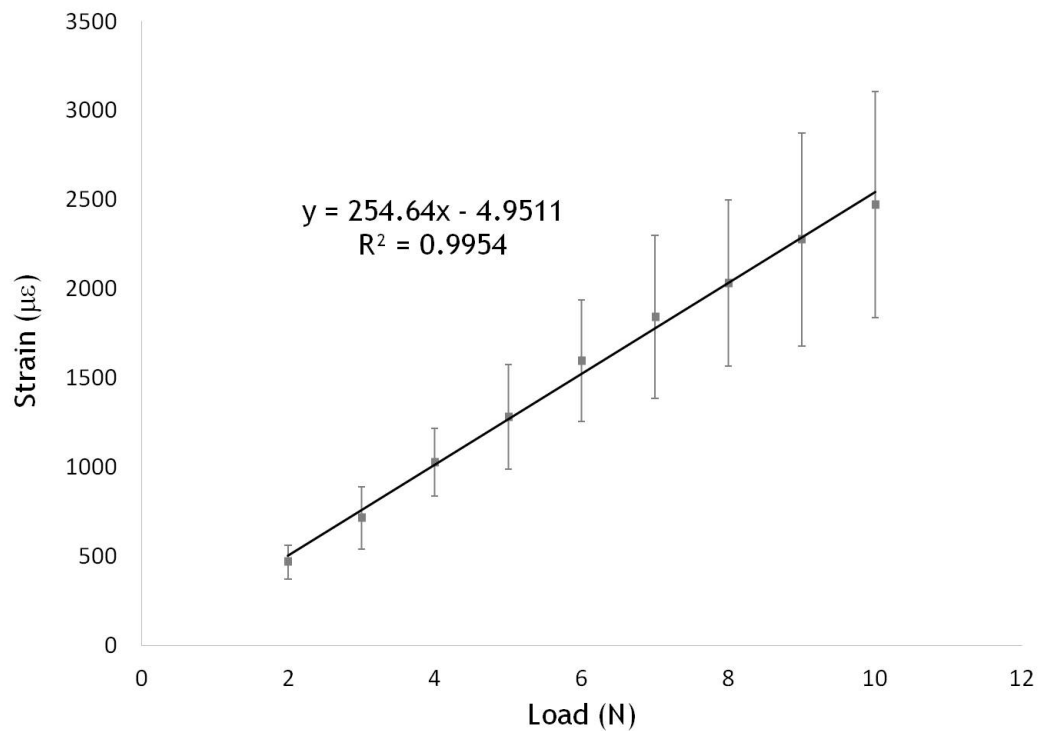
Fig. 2.5. Strain-load calibration determined by applying strain gauges to five mouse hind limbs ex vivo.

2.2.2   Micro Computed Tomography

The sample size for cortical analysis was n = 22 per group with the exception of the loaded BAPN group, which had n = 21 due to a bone breaking during harvest. All measured parameters were statistically analysed looking at the main effects of loading and disease. The results from the cortical analysis are shown in Table 2.1. It was found that cortical area (p = 0.0206) and cortical thickness (p<0.0001) significantly increased as an effect of loading. The only effect of disease was a significant increase in TMD (p = 0.0288), which indicates that the bones from BAPN treated mice were more highly mineralized than PBS treated mice.

Table 2.1
Cortical Analysis from μCT

	Total CSA (mm²)	Marrow Area (mm²)	Cortical Area (mm²)*	Cortical Thickness (mm)*	TMD (g/cm³)†
Non-Loaded PBS	0.85 ± 0.06	0.32 ± 0.03	0.53 ± 0.03	0.20 ± 0.004	1.81 ± 0.02
Loaded PBS	0.86 ± 0.06	0.31 ± 0.04	0.55 ± 0.03	0.21 ± 0.01	1.81 ± 0.03
Non-Loaded BAPN	0.86 ± 0.05	0.32 ± 0.03	0.54 ± 0.03	0.20 ± 0.01	1.82 ± 0.03
Loaded BAPN	0.87 ± 0.06	0.31 ± 0.04	0.55 ± 0.03	0.21 ± 0.01	1.83 ± 0.02

*indicates a significant difference (p<0.05) between non-loaded and loaded tibiae
†indicates a significant difference (p<0.05) between PBS and BAPN treated tibiae

For the trabecular analysis, main effects of loading included a significant increase in trabecular thickness (Tb.Th, p<0.0001) paired with a significant decrease in trabecular number (Tb.N, p = 0.0066). Additionally, the structural modelling index (SMI) was increased with loading (p<0.0001), indicating that the trabecular struts were shaped more like rods than plates. Trabecular parameters are shown in Table 2.2. There were no effects of BAPN treatment on any parameter. There were also no significant interaction terms for either cortical or trabecular analyses.

Table 2.2
Trabecular Analysis from μCT

	MS/BS (%)	Tb.Th (μm)*	Tb.Sp (μm)	Tr.N (1/mm)*	SMI*
Non-Loaded PBS	4.46 ± 0.90	71.6 ± 3.7	460 ± 32	0.63 ± 0.12	2.64 ± 0.13
Loaded PBS	4.31 ± 0.80	76.7 ± 3.4	472 ± 46	0.56 ± 0.11	2.78 ± 0.11
Non-Loaded BAPN	5.15 ± 1.30	73.2 ± 2.6	472 ± 36	0.70 ± 0.17	2.58 ± 0.12
Loaded BAPN	4.40 ± 0.80	76.1 ± 3.6	480 ± 34	0.58 ± 0.11	2.71 ± 0.12

*indicates a significant difference (p<0.05) between non-loaded and loaded tibiae

Cortical bone profiles were generated by plotting the radii from the centroid to both the endocortical and periosteal surfaces at 0.5 degree angular increments for all bones and then averaged for each group. These profiles qualitatively demonstrate where bone modeling due to loading is occurring. For both PBS (Figure 2.6A) and BAPN (Figure 2.6B) injected mice, geometric changes occurred in loaded bones on the same locations of the periosteal and endocortical surfaces but there was not a robust formation response.
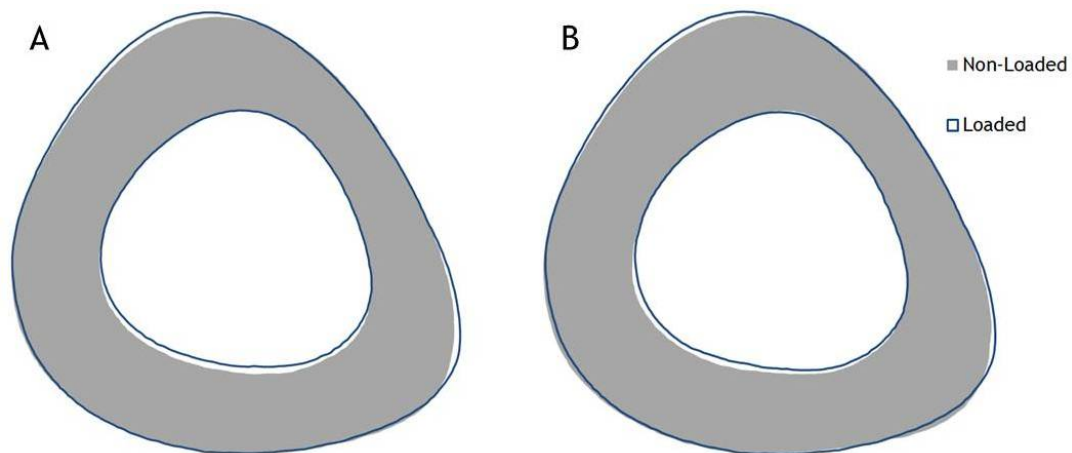
Fig. 2.6. Cortical perimeters reconstructed from μCT geometric data for non-loaded and loaded bones within a. PBS injected mice and b. BAPN injected mice.

2.2.3 Whole Bone Mechanical Testing

One-half of the 88 tibiae analysed using CT were tested to failure in four-point bending, n = 11 per group. After the failure tests, five bones were excluded from analysis as statistical outliers. The sample size for PBS injected mice remained n = 11, and the BAPN mice were reduced to sample sizes of n = 9 for non-loaded and n = 8 for loaded bones. There were no significant interaction effects for any four-point bending parameter. Structural mechanical properties are shown in Tables 2.3 and 2.4. Deformation to yield (p = 0.0343) and work to yield (p = 0.0023) increased with loading. There were no main effects of disease, however there was a trending increase in preyield work (p = 0.07) in diseased animals.

Table 2.3
Preyield Structural Mechanical Properties from Four-Point Bending to Failure

	Yield Load (N)	Stiffness (N/mm)	Deformation to Yield (μm)*	Work to Yield (mJ)*
Non-Loaded PBS	11.4 $\pm$ 1.2	60.1 $\pm$ 11.0	216 $\pm$ 44	1.35 $\pm$ 0.29
Loaded PBS	12.7 $\pm$ 1.0	55.8 $\pm$ 14.3	271 $\pm$ 78	1.86 $\pm$ 0.54
Non-Loaded BAPN	12.1 $\pm$ 0.6	53.6 $\pm$ 5.9	248 $\pm$ 23	1.64 $\pm$ 0.20
Loaded BAPN	13.0 $\pm$ 0.7	52.7 $\pm$ 6.2	285 $\pm$ 80	2.03 $\pm$ 0.59

*indicates a significant difference (p<0.05) between non-loaded and loaded tibiae

Tables 2.5 and 2.6 show tissue-level mechanical properties. There was a significant increase in yield stress (p = 0.0369) and resilience (p = 0.0092) due to loading. The only effect of disease was a significant increase in strain to yield (p = 0.0441).

Table 2.4

Postyield Structural Mechanical Properties from Four-Point Bending to Failure

	Ultimate Load (N)	Postyield Displacement (μm)	Total Deformation (μm)	Postyield Work (mJ)	Work to Failure (mJ)*
Non-Loaded PBS	14.6 ± 2.0	694 ± 232	911 ± 224	8.8 ± 3.3	10.2 ± 3.3
Loaded PBS	14.6 ± 0.9	691 ± 158	962 ± 155	8.9 ± 2.1	10.7 ± 2.0
Non-Loaded BAPN	15.4 ± 2.7	762 ± 99	1010 ± 117	9.5 ± 1.6	11.2 ± 1.7
Loaded BAPN	14.5 ± 0.7	732 ± 215	1017 ± 166	9.5 ± 2.6	11.6 ± 2.3

Table 2.5

Preyield Tissue-Level Mechanical Properties from Four-Point Bending to Failure

	Yield Stress (MPa)*	Elastic Modulus (MPa)	Strain to Yield ($\mu\epsilon$)†	Resilience (MPa)*
Non-Loaded PBS	167 ± 45	10.8 ± 3.4	17613 ± 3345	1.60 ± 0.49
Loaded PBS	202 ± 50	11.9 ± 3.8	20009 ± 5248	2.20 ± 0.75
Non-Loaded BAPN	168 ± 27	9.4 ± 2.2	19945 ± 2430	1.81 ± 0.28
Loaded BAPN	193 ± 43	10.0 ± 2.9	22468 ± 6647	2.35 ± 0.81

*indicates a significant difference (p<0.05) between non-loaded and loaded tibiae
†indicates a significant difference (p<0.05) between PBS and BAPN treated tibiae

Table 2.6

Postyield Tissue-Level Mechanical Properties from Four-Point Bending to Failure

	Ultimate Stress (MPa)	Strain to Failure ($\mu\epsilon$)	Toughness (MPa)
Non-Loaded PBS	214 ± 63	75114 ± 22713	12.8 ± 7.4
Loaded PBS	230 ± 48	71401 ± 10344	12.6 ± 3.4
Non-Loaded BAPN	217 ± 60	81247 ± 11753	12.4 ± 2.5
Loaded BAPN	215 ± 46	80015 ± 13246	13.4 ± 3.4

2.2.4   Fracture Toughness

The remaining tibiae from the μCT analyses that were not tested to failure in four-point bending were used to determine fracture toughness (n = 11 per group). Four bones were lost during notching, so the sample sizes analysed were n = 10 for non-loaded PBS, n = 11 for loaded PBS, n = 9 for non-loaded BAPN, and n = 10 for loaded BAPN. Fracture stress intensity (K) was calculated using three different forces obtained from the three-point bending tests [6]. K initiation was calculated using the yield force and notch angle. K max load was calculated using the ultimate force and notch angle. K unstable was calculated using failure load and instability angle. All three calculated values are shown in Table 2.7. The only significant difference was a significant decrease in K max load with loading (p = 0.0181). There were no significant effects of disease or interactions.

2.2.5   Raman Spectroscopy

Forty bones (n = 10 per group) were used to evaluate molecular composition via Raman spectroscopy. The results are shown in Table 2.8. There was no significant effect of loading for any property. The three mineral-to-matrix ratios, MMR Amide I (p = 0.0181), MMR Amide III (p = 0.019), and MMR CH2 (p = 0.0223), were all

Table 2.7
Fracture Toughness

	K, initiation	K, max load*	K, unstable
Non-Loaded PBS	4.10 ± 0.57	5.30 ± 0.38	5.73 ± 0.97
Loaded PBS	3.98 ± 0.39	4.85 ± 0.66	5.21 ± 1.01
Non-Loaded BAPN	4.24 ± 0.38	5.32 ± 0.51	5.69 ± 0.99
Loaded BAPN	3.95 ± 0.23	5.01 ± 0.26	5.67 ± 0.67

*indicates a significant difference ($p<0.05$) between non-loaded and loaded tibiae

significantly increased due to disease, indicating higher mineralization of bone tissue in BAPN injected animals. Amide I/Amide III, an indicator of secondary structure stability, had a significant interaction term ($p = 0.0046$). The subsequent one-way ANOVA had a p-value of 0.0108, indicating that post hoc Tukeys HSD tests could be used to compare groups. The result was that within the loaded groups, there was a significant effect of BAPN ($p = 0.005$), and within the BAPN groups there was a significant decrease due to loading ($p = 0.0004$).

2.2.6 Reference Point Indentation

The same forty bones used for Raman spectroscopy were intended for reference point indentation. Two bones were lost during RPI testing and one bone was lost due to improper storage between Raman and RPI tests. Therefore the sample sizes used for RPI were $n = 10$ non-loaded PBS, $n = 9$ loaded PBA, $n = 9$ non-loaded BAPN, and $n = 9$ loaded BAPN. The results are shown in Table 2.9. There were no significant effects of disease or interactions. There were also no significant effects of loading either, although total energy ($p = 0.0812$), average CID ($p = 0.0796$), and energy dissipation ($p = 0.0679$) all had trending decreases.

Table 2.8
Raman Spectroscopy

	Crystallinity	MMR Amide I†	Carbonate/ Phosphate	MMR Amide III†	MMR CH2†	Amide I/Amide III#
Non-Loaded PBS	0.051 ± 0.002	1.12 ± 0.30	0.37 ± 0.05	1.75 ± 0.32	2.25 ± 0.39	1.62 ± 0.22
Loaded PBS	0.050 ± 0.002	0.99 ± 0.20	0.38 ± 0.05	1.63 ± 0.28	2.12 ± 0.34	1.72 ± 0.22^{b}
Non-Loaded BAPN	0.051 ± 0.001	1.21 ± 0.24	0.34 ± 0.04	1.99 ± 0.38	2.56 ± 0.41	1.68 ± 0.09^{a}
Loaded BAPN	0.051 ± 0.002	1.28 ± 0.26	0.35 ± 0.05	1.91 ± 0.34	2.39 ± 0.42	1.48 ± 0.12

† indicates a significant difference ($p<0.05$) between PBS and BAPN treated tibiae

\# indicates an interaction effect ($p<0.05$)

a indicates a significant post hoc effect ($p<0.05$) compared to loaded tibiae of the same disease state

b indicates a significant post hoc effect ($p<0.05$) compared to BAPN treated tibiae of the same load state

Table 2.9
Reference Point Indentation

	ID(1st) (μm)	IDI (μm)	TID (μm)	Total Energy (μJ)	Average CID (μm)	Energy Dissipation (μJ)	Unloading Slope (N/μm)
Non-Loaded PBS	39.0 ± 5.0	8.3 ± 2.9	43.8 ± 6.4	92.1 ± 22.8	1.9 ± 0.6	6.2 ± 2.0	0.18 ± 0.02
Loaded PBS	35.6 ± 2.8	6.8 ± 1.5	39.4 ± 3.3	77.1 ± 8.0	1.5 ± 0.2	5.1 ± 0.7	0.19 ± 0.02
Non-Loaded BAPN	37.2 ± 3.7	7.1 ± 1.3	41.1 ± 3.8	87.7 ± 13.7	1.7 ± 0.3	5.9 ± 1.1	0.17 ± 0.02
Loaded BAPN	38.0 ± 4.4	7.0 ± 1.0	41.7 ± 5.5	82.8 ± 7.3	1.6 ± 0.3	5.4 ± 0.6	0.18 ± 0.02

2.2.7 Fatigue

Forty bones were fatigued, n = 10 per group. Three bones broke during the fatigue test and three more were excluded from the analysis due to incomplete data sets obtained from the testing machine. The sample sizes per group were n = 9 non-loaded PBS, n = 10 loaded PBS, n = 7 non-loaded BAPN, and n = 8 loaded BAPN. Stiffness was calculated from single load-unload curves obtained just prior to the start of and immediately after the conclusion of fatigue. Using a repeated measures ANOVA looking at the effects of loading, disease, and fatigue, it was found that there was a significant increase in stiffness due to fatigue ($p < 0.0001$) (Figure 2.7).
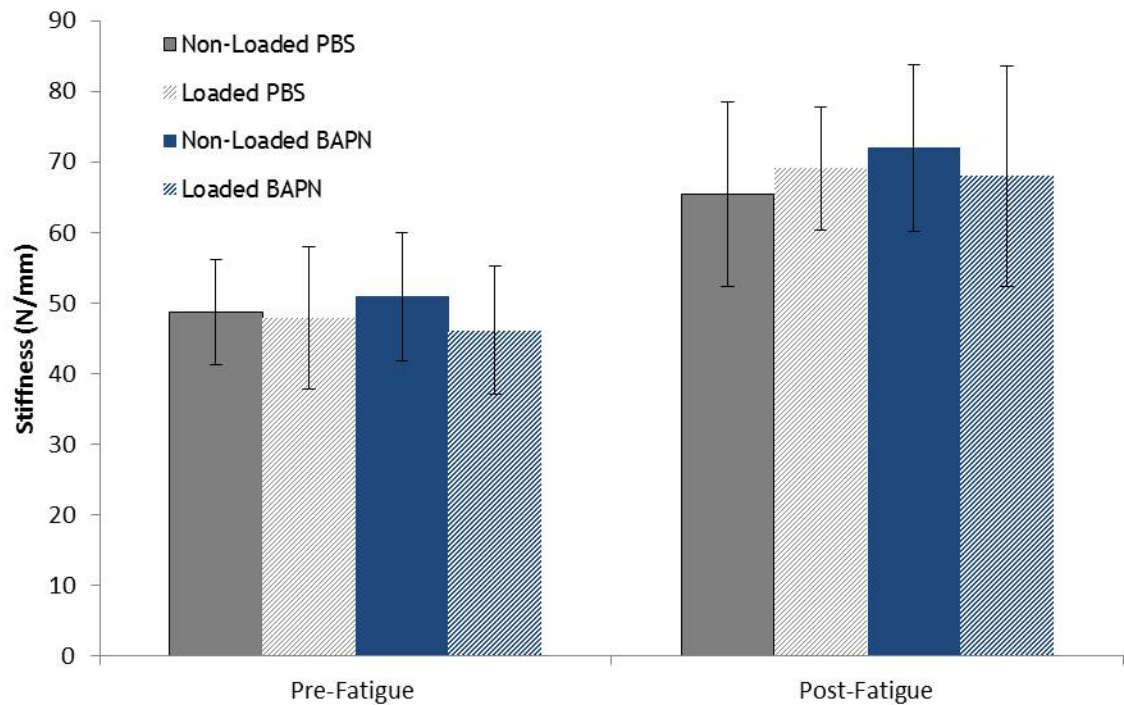
Fig. 2.7. Stiffness values obtained from load-unload curves before and after fatigue.There were no significant effects of loading or disease. There was a significant increase as a main effect of fatigue.

2.2.8 Histomorphometry and Microdamage Analysis

The thirty-four tibiae used to analyse change in stiffness and forty additional non-fatigued tibiae were stained and processed for histomorphometric and microdamage analyses. These bones all came from animals that were given in vivo calcein injections. Ten bones were damaged or lost during processing. Additionally, there were some cases where only 3 sections could be obtained from an embedded block or all sections obtained were not measurable due to the grinding process required for histomorphometry. In those cases, the bones were only used for microdamage analysis and excluded from histomorphometry, with the exception of one bone which was used for histomorphometry and not microdamge because two of the sections had already been ground. For histromorphometry, non-fatigued and fatigued bones were pooled together, reducing 8 groups to 4 because fatigue has no effect on histomorphometry indices since the labels were given in vivo prior to ex vivo fatigue. Further exclusions were made when no calcein label was present on either the periosteal or endocortical surfaces of all 6 sections as it was not possible to determine if no label was present as a function of bone remodelling or if no label was present due to failed calcein injections during loading, leading to 11 additional exclusions. The final sample sizes for histomorphometric analysis were n = 13 non-loaded PBS, n = 11 loaded PBS, n = 16 non-loaded BAPN, and n = 12 loaded BAPN. These sample sizes further reduced for calculations of MAR and BFR. If labels were present but none were double labels, it was not possible to calculate an Ir.L.W. In this case, MAR and BFR are both zero values and were excluded from analysis as they would skew the resulting means. Reduced sample sizes for these measures are shown alongside the data in Tables 2.10 and 2.11. The only detectable effect of loading was a significant increase in endocortical MS/BS. There were no effects of disease or interactions.

Sample size for microdamage analysis were n = 10 non-fatigued/non-loaded PBS, n = 8 fatigued/non-loaded PBS, n = 7 non-fatigued/loaded PBS, n = 10 fatigued/loaded PBS, n = 10 non-fatigued/non-loaded BAPN, n = 7 fatigued/non-loaded BAPN, n

Table 2.10
Histomorphometry of Periosteal Surface

	MS/BS (%)	Reduced Sample Size (n)	MAR (μm/day)	BFR/BS (μm/day)
Non-Loaded PBS	13.6 ± 9.3	4	0.9 ± 0.3	17.8 ± 15.3
Loaded PBS	15.4 ± 15.6	2	0.7 ± 0.007	31.7 ± 4.4
Non-Loaded BAPN	14.8 ± 11.3	5	1.1 ± 0.4	22.5 ± 25.3
Loaded BAPN	18.0 ± 11.0	4	0.9 ± 0.6	27.3 ± 21.8

Table 2.11
Histomorphometry of Endocortical Surface

	MS/BS (%)*	Reduced Sample Size (n)	MAR (μm/day)	BFR/BS (μm/day)
Non-Loaded PBS	48.1 ± 17.0	7	1.1 ± 0.2	62.4 ± 18.8
Loaded PBS	56.4 ± 16.9	6	1.2 ± 0.2	82.4 ± 38.1
Non-Loaded BAPN	46.1 ± 20.1	8	1.3 ± 0.3	80.0 ± 34.3
Loaded BAPN	65.0 ± 22.8	9	1.2 ± 0.6	87.3 ± 60.6

*indicates a significant difference ($p<0.05$) between non-loaded and loaded tibiae

= 9 non-fatigued/loaded BAPN, n = 8 fatigued/loaded BAPN. Upon analysis, it was discovered that no microcracks were present in any of the non-fatigued bones, so these groups were excluded from the analysis. The remaining groups were first analysed including all samples, and it was found that no significant effects of loading or disease occurred. The analysis was then repeated after excluding bones in which there was no damage, reducing the sample sizes to n = 4 fatigued/non-loaded PBS, n = 5 fatigued/loaded PBS, n = 5 fatigued/non-loaded BAPN, and n = 5 fatigued/loaded BAPN. The data from this analysis is shown in Table 2.12.

Table 2.12

Microdamage Analysis of Fatigued Tibiae

	Cr.N (#)*	Cr.L (μm)*	Cr.D (#/mm²)*	Cr.S.D (μm/mm²)*
Non-Loaded PBS	15.5 ± 13.3	472 ± 474	15.7 ± 13.1	478 ± 468
Loaded PBS	2.5 ± 3.5	74 ± 109	2.5 ± 3.6	75 ± 111
Non-Loaded BAPN	9.6 ± 5.9	254 ± 150	9.7 ± 5.9	254 ± 142
Loaded BAPN	4.8 ± 4.3	88 ± 109	4.8 ± 4.1	88 ± 105

*indicates a significant difference (p<0.05) between non-loaded and loaded tibiae

While there were no effects of disease, Cr.N (p = 0.0452), Cr.Le (p = 0.0186), Cr.D (p = 0.0407) and Cr.S.D (p = 0.0166) all significantly decreased due to loading, indicating that in vivo loading protected the tibiae against microdamage formation caused by ex vivo fatigue.

2.3   Discussion

The goals of this study were two-fold: to evaluate the effect of in vivo tibial loading on geometric, molecular, and mechanical properties, and to investigate the ability of the in vivo tibial loading model to mitigate the effects of a bone disease, in this case osteolathrysm. Therefore, a low strain level of 1750 $\mu\epsilon$ was chosen, as higher strain levels have been shown to induce osteoarthritis in a murine model [7].

The effects of loading on cortical bone were small, with slight increases in both cortical area and thickness, indicating that any detectable changes in mechanical properties are due to changes in pre-existing bone rather than newly formed bone. Additionally, the increase in cortical area paired with no change in total cross-sectional area indicates that any change in geometry is primarily driven by the endocortical surface, which was supported by both the perimeter profiles and histomorphometric analysis in which the presence of labels, particularly double labels, was on the endo-

cortical surface. The trabecular response was that loading resulted in fewer, thicker, rod-like trabeculae. These cortical and trabecular changes indicate that while the expected robust changes in geometric structure were not present, some bone modelling was occurring. Perhaps loading for a longer period of time (more total days of loading) would drive an increased geometric response. These findings are consistent with a concurrent multistrain study, discussed in the next chapter. Histomorphometry failed to identify significant effects of loading, however this is likely due to the small sample sizes analyzed. The question of whether the reductions of sample size were driven by ineffective injections or the absence of bone growth cannot be definitively answered, but based on the presence of labels in some samples within all groups and the small cortical differences it is likely due to lack of growth. There was a significant increase in endocortical mineralizing surface, the parameter with the largest sample sizes per group, but no change in periosteal mineralizing surface.

As expected based on the lack of robust geometric change, there were limited effects of loading on mechanical parameters. Preyield mechanical properties were significantly affected by loading, driven purely by changes in the yield point. There was no significant change in stiffness or elastic modulus, however the structural mechanical property deformation to yield increased and because yield force did not change, likely drove an increase in work to yield as well. Interestingly, though not translated to structural mechanical properties as a change in yield force, yield stress significantly increased due to loading and likely drove the increase in resilience. Yield stress is a tissue-level property, and a change here paired with little change in geometry is evidence of a change in quality of pre-existing tissue. It is important to note that while not statistically significant the means of both yield force and strain to yield were increased by 9% and 13%, respectively, in the loaded groups compared to non-loaded. Therefore it cannot be said that the change in deformation to yield alone drove the other changes in structural and tissue-level mechanical properties.

Three measures of fracture toughness were calculated and though all three trended down, the only significant effect of loading was a decrease in K max force. This would

indicate that loading decreased the ability of the bone to resist fracture, a negative impact, and is supported by trending decreases in total energy dissipation, average energy dissipation, and creep from reference point indentation, though none were significant. In contrast, microdamage analysis showed that while fatigue-induced microcracks formed in a majority of bones, and even formed in more total bones in the loaded verses control limbs (60% non-loaded vs. 67% loaded) the number and length of these cracks decreased with in vivo loading, even when normalized to cortical area. This could be explained by the trending decrease in stiffness with loading, though significance was not reached. The absence of microdamage in non-fatigued bones indicates that in vivo loading was not detrimental on its own and all cracks formed were due to fatigue. Therefore, loading did not equip bones to resist fatigue-induced damage completely, but did reduce the severity of damage formation.

The effects of BAPN treatment were few. Tissue mineral density was increased in the BAPN group, indicating that more mineral was present in those bones. In agreement with this measure, all three MMR ratios from Raman spectroscopy were increased with BAPN. This suggests that there is some BAPN-induced change in collagen structure allowing for mineralization to occur in greater quantity around and between fibrils, such as an increase in spacing between fibrils as a result of reduced cross-linking. The only other effect of BAPN treatment was an increase in strain to yield, though this was not translated to the structural property of deformation to yield. There was a trending increase in pre-yield work with BAPN (p = 0.07) that did not reach significance. The overall absence of influence of reduced cross-linking on mechanical outcomes suggests that the treatment was not successful in altering bone structure. Despite the fact that this age and sex of mouse should be undergoing rapid growth, this lack of BAPN-induced effects is likely due to little bone growth occurring, since BAPN only interrupts newly formed cross-links and does not affect pre-existing tissue. This indicates that in order to affect more tissue, BAPN injections should be carried out over a longer period of time or a higher strain level must be

used to induce more bone growth in order to successfully create a diseased state of bone.

There were several limitations to this study. Because bone is rapidly forming at 8 weeks of age, it is possible that in order to overcome expected growth due to aging over the loading period, a higher strain level needs to be used. The lack of a baseline group used in this study prevented comparisons between bone geometry at the start of loading to the non-loaded tibiae to isolate growth due to age from growth induced by loading. A second limitation was that using a scanning resolution of 17 μm in order to scan the entire bone eliminated the ability of accurately measuring trabecular bone mineral density, which is why it is absent from the results. Additionally, bending and fatiguing in a four-point bending set-up is not physiological. It would be more accurate to perform these tests in an axial compression set-up, however as previously mentioned preliminary work investigating testing in this orientation resulted in a majority of the tibiae failing at or just distal to the growth plate, which could be due to the growth plates of these young animals not being entirely fused, creating a weaker bone cross-section at that location. The young age of animals chosen also limited the number of locations used in Raman spectroscopy and RPI analysis due to the short region of bone available for these tests. An additional limitation is the lack of assays measuring cellular activity and contributions to the measured effects on bone growth. While this was outside the scope of this study, future studies should consider cellular effects, as they are important to understanding the relationship between in vivo mechanical stimulation and bone adaptation.

In conclusion, while there was not an overwhelming response of the bone tissue due to loading, the ability of a short loading experiment to a low strain level to provide protection against the formation of microcracks is promising feedback. In addition, there was no outward signs, in terms of animal behavior, that loading to these levels induced pain or joint damage. Trends in geometric and mechanical properties indicate that higher strain levels or a longer loading experiment may result in the hypothesized bone response. Therefore, the next step was to determine what strain level is required

to engender a robust bone formation response due to loading in young, rapidly growing mice. This is addressed in the next chapter.

2.4   References

[1] R. P. Main, M. E. Lynch, and M. C. H. van der Meulen, "In vivo tibial stiffness is maintained by whole bone morphology and cross-sectional geometry in growing female mice," *Journal of Biomechanics*, vol. 43, no. 14, pp. 2689–2694, 2010.

[2] J. M. Wallace, K. Golcuk, M. D. Morris, and D. H. Kohn, "Inbred strain-specific response to biglycan deficiency in the cortical bone of c57bl6/129 and c3h/he mice," *Journal of Bone and Mineral Research*, vol. 24, no. 6, pp. 1002–1012, 2009.

[3] R. O. Ritchie, K. J. Koester, S. Ionova, W. Yao, N. E. Lane, and J. W. Ager, "Measurement of the toughness of bone: A tutorial with special reference to small animal studies()," *Bone*, vol. 43, no. 5, pp. 798–812, 2008.

[4] M. A. Hammond, M. A. Gallant, D. B. Burr, and J. M. Wallace, "Nanoscale changes in collagen are reflected in physical and mechanical properties of bone at the microscale in diabetic rats," *Bone*, vol. 60, no. 0, pp. 26–32, 2014.

[5] Z. R. Bart, M. A. Hammond, and J. M. Wallace, "Multi-scale analysis of bone chemistry, morphology and mechanics in the oim model of osteogenesis imperfecta," *Connective Tissue Research*, vol. 55, no. S1, pp. 4–8, 2014.

[6] R. O. Ritchie, K. J. Koester, S. Ionova, W. Yao, N. E. Lane, and J. W. Ager, "Measurement of the toughness of bone: A tutorial with special reference to small animal studies()," *Bone*, vol. 43, no. 5, pp. 798–812, 2008.

[7] F. C. Ko, C. Dragomir, D. A. Plumb, S. R. Goldring, T. M. Wright, M. B. Goldring, and M. C. van der Meulen, "In vivo cyclic compression causes cartilage degeneration and subchondral bone changes in mouse tibiae," *Arthritis Rheum*, vol. 65, no. 6, pp. 1569–78, 2013.

3. MULTISTRAIN TIBIAL LOADING STUDY

The following chapter was submitted as a paper with the title *Cortical and Cancellous Structural Adaptation and Improvements to Mechanical Integrity are Strain Dependent with Axial Compression of the Tibia in Female C57BL/6 Mice* to PLOS ONE on February 2015 in its entirety and is currently under review. Authors on the paper, in the order listed, were Alycia G. Berman (co-first author), Creasy A. Clauser (co-first author), Caitlin Wunderlin, Max A. Hammond, and Joseph M. Wallace (corresponding author).

3.1 Abstract

Strain-induced adaption of bone has been well-studied in an axial loading model of the mouse tibia. However, most outcomes of these studies are restricted to changes in bone architecture and do not explore the mechanical implications of those changes. Herein, we studied both the mechanical and morphological adaptions of bone to three strain levels using a targeted tibial loading mouse model. We hypothesized that loading would increase bone architecture and improve mechanical properties in a dose-dependent fashion. The right tibiae of female C57BL/6 mice (8 week old) were compressively loaded for 2 weeks to one of three strain levels (1700 $\mu\epsilon$, 2050 $\mu\epsilon$, and 2400 $\mu\epsilon$ as determined by a strain calibration), while the left limb served as an non-loaded control. Following loading, ex vivo analyses of bone architecture and mechanical integrity were assessed by micro-computed tomography and 4-point bending. Results indicated that loading improved bone architecture in a dose-dependent manner and improved mechanical outcomes at 2050 $\mu\epsilon$. Loading to 2050 $\mu\epsilon$ resulted in a strong and compelling formation response in both cortical and cancellous regions. In addition, both structural and tissue level strength and energy dissipation were posi-

tively impacted. Loading to the highest strain level also resulted in rapid and robust formation of bone in both cortical and cancellous regions. However, these improvements came at the cost of a woven bone response in half of the animals. Loading to the lowest strain level had little effect on bone architecture and failed to impact structural- or tissue-level mechanical properties. Potential systemic effects were identified for trabecular tissue mineral density, bone volume fraction, and in the pre-yield region of the force-displacement and stress-strain curves. Future studies will focus on a moderate load level which was largely beneficial in terms of cortical/cancellous structure and mechanical function.

3.2 Introduction

Bone is a dynamic hierarchical material that spans several orders of magnitude in length scale [1]. Bone has been shown to adapt its chemical makeup and structural organization in response to mechanical stimulation across these hierarchical length scales. Rodent models are often used to study specific aspects of bones adaptive response to loading. Exercise models including jumping, swimming, and running have been used as effective loading models in mice and rats with well-documented effects on skeletal structure and function [2–6]. These models have the advantage of being simplistic in design and physiologically relevant. However, in addition to whole body systemic effects, they prevent having control over loading parameters such as load/strain stimulus, cyclic design, and orientation of loading. Direct loading of individual limbs overcomes these obstacles and provides a way to control all aspects of loading to focus on the mechanisms underlying a response to specific mechanical cues.

The ulnar loading model has been successfully used for more than 15 years to study the response to loading in mice and rats [7–9]. More recently, axial loading of the mouse tibia has become a well-accepted model and has provided insight into the effects of loading as a function of age [10–18], sex [19–21], inbred strain [22],

disease [23–26], fracture healing [27, 28], and load/strain level [29–33]. Interestingly, despite the increasing use of tibial loading in mice, few studies have placed significance on mechanical outcomes. One study looked at mechanics in a fracture healing model, where the fracture site was directly loaded [28]. A second study performed axial loading to failure following a 6 week tibial loading experiment and reported an increase in structural mechanical properties [22]. A third study indirectly calculated elastic modulus by assuming a relationship between ash mineral density and the attenuation coefficient obtained from micro-computed tomography (μCT) [18].

The majority of studies have investigated the effect of tibial loading on bone formation using dynamic histomorphometry and/or μCT. These outcomes are important to assess how and where bone forms in response to loading. However, if changes in formation fail to improve functional properties of the bone, an increase in bone formation could be less compelling. For example, if more bone is formed due to loading, but that bone is not better equipped to bear load or resist fracture, loading did not achieve a beneficial functional outcome. For this reason, it is important to investigate mechanical outcomes alongside formation.

To remain consistent with the majority of tibial loading studies, female C57BL/6 mice were used here. Although studies have used this strain of mice with starting ages ranging from 8 weeks to 19 months, we chose to use mice at 8 weeks of age to be consistent with previous studies in our lab utilizing treadmill running [34–36]. The goal of this study was to investigate the mechanical implications of targeted in vivo loading in addition to changes in cortical and trabecular architecture. We hypothesized that loading in female mice would lead to dose-dependent increases in cortical and trabecular architectural parameters as well as increased mechanical stiffness, strength, and ductility.

3.3 Materials and Methods

3.3.1 Animals

Animals (n = 35, female, C57BL/6NHsd) were obtained from Harlan Laboratories (Indianapolis, IN) at approximately 7 weeks of age and allowed to acclimate for one week prior to the start of in vivo loading. Animals were handled following Indiana University School of Science Institutional Animal Care and Use Committee (IACUC) approval (SC210R) and group-housed with access to food and water ad libitum in a light/dark controlled room. Body mass was recorded two days prior to the beginning of loading and animals were randomly sorted into weight-matched groups (three groups of 10 for loading, one group of 5 for calibration). Animals were weighed every other day after the start of loading to assess overall health.

3.3.2 Strain Calibration

One day prior to beginning in vivo loading, five mice were sacrificed via CO_2 inhalation. Immediate after sacrifice, a small incision was made through the skin of the right tibia and the skin was retracted in order to attach a single-element microstrain gauge (Vishay, Shelton, CT: EA-06-015DJ-120) to the anteromedial surface of the bone, proximal to the tibia-fibula junction. The exposed bone surface was first cleaned using chloroform and the gauge was attached using an adhesive kit (M-Bond 200). After briefly drying, the gauge was coated with polyurethane (M-Coat A) and the skin was released to cover the wound. Using a mechanical testing machine (Bose Corporation, Eden Prairie, MN: Electroforce 3200) equipped with a 45 N load cell and a custom loading fixture, the tibiae were loaded using a 2 Hz haversine waveform and load was stepped up from 2 N to 12 N in 1 N increments. Load and strain were recorded simultaneously. Load versus strain curves were plotted and a linear fit was applied to obtain the relationship between load and strain. Using this calibration

curve, it was determined that to achieve 1700 $\mu\epsilon$, 2050 $\mu\epsilon$, and 2400 $\mu\epsilon$, applied loads of 8.8 N, 10.6 N, and 12.4 N were needed, respectively.

3.3.3 In Vivo Loading

The three remaining groups of mice (n = 10 each) were randomly assigned to low strain, mid strain, and high strain loading. Isoflurane-induced anesthesia (2%) was used to anesthetize mice prior to loading and mice were maintained under anesthesia for the duration of loading. Right tibiae were loaded (cyclic compression, 2 Hz) over a 14 day period with a day of rest after every third day of loading, resulting in 9 loading days (Figure 3.1A). The loading profile consisted of four haversine waveforms followed by 3 seconds of rest repeated 55 times for a total of 220 cycles of loading per day (Figure 3.1B). After the final bout of loading, mice were allowed to rest for two days before sacrifice. Animals were euthanized at 10 weeks of age via CO_2 inhalation. Right and left tibiae were harvested, total length was measured using calipers, and each bone was wrapped in phosphate buffered saline (PBS)-soaked gauze and stored at -20 °C.
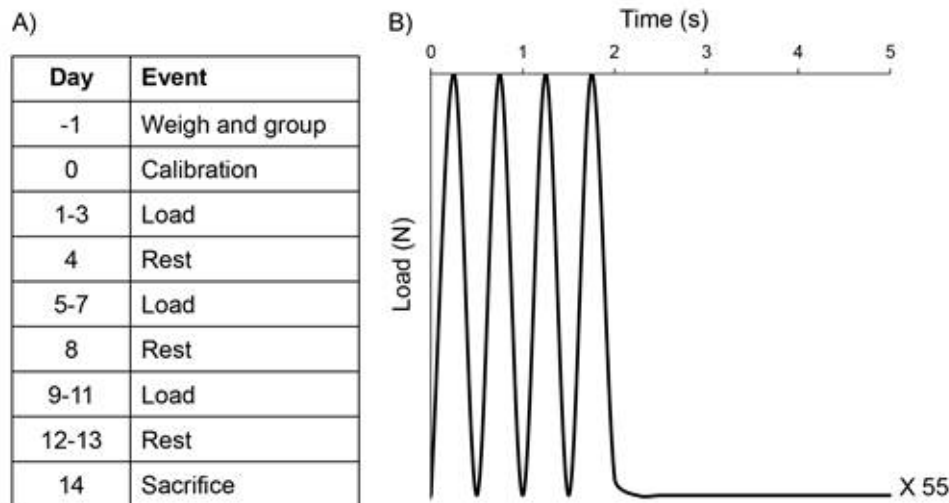
Fig. 3.1. Timeline for tibial loading study and waveform profile. A) The right tibia of each mouse was loaded using the waveform to a set force (8.8 N, 10.6 N and 12.4 N) to elicit a desired strain level (1700 $\mu\epsilon$, 2050 $\mu\epsilon$ and 2400 $\mu\epsilon$) over a 14 day period. B) The loading profile consisted of four haversine waveforms followed by 3 seconds of rest repeated 55 times for a total of 220 cycles of loading per day.

3.3.4 Micro Computed Tomography (μCT)

All tibiae were scanned using a high-resolution CT system (Bruker-MicroCT, Kontich, Belgium; Skyscan 1172). Calibration was performed daily prior to scanning the bones using two cylindrical hydroxyapatite phantoms (0.25 and 0.75 g/cm3 CaHA). Scans were performed on hydrated bones with the long axis oriented vertically at an isotropic voxel size of 10.2 μm resolution (V = 60 kV, I = 167 μA), then reconstructed for use in cortical and trabecular analyses. For cortical bone analysis, a standard diaphyseal site was chosen 45% of the bones total length away from the proximal growth plate (Figure 3.2). Seven transverse slices were obtained from this site and converted to binary images with a grayscale threshold value of 75. Cortical geometric properties and tissue mineral density (TMD) were obtained from these images. Trabecular analysis was performed on 12% of the total bone length in the proximal metaphysis starting at the distal end of the growth plate. Regions of interest including only can-

cellous bone were automatically segmented using a custom Matlab code. Parameters of trabecular architecture and TMD were obtained.
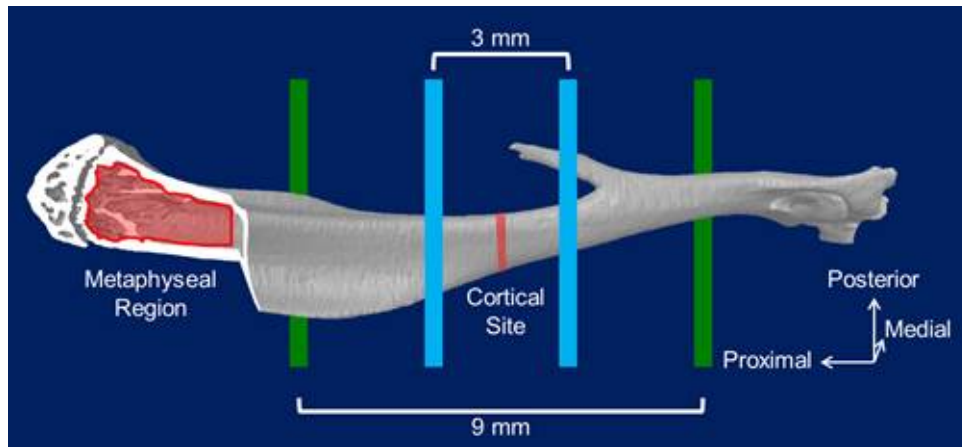
Fig. 3.2. Location of mechanical tests and micro-computed tomography (μCT) regions of interest. The diaphysis of each bone was loaded using 4-point bending with the medial surface in tension. The bottom support points (green) were located 9 mm apart and the top loading points (blue) were located 3 mm apart. The metaphyseal region used for trabecular analyses began just distal to the growth plate in the proximal metaphysis and extended distally by 12% of the overall bone length. The cortical standard site was located 45% the total bone length from the proximal growth plate. Strain gauges used for calibration were in the region spanning the cortical standard site on the anteromedial surface.

3.3.5   Mechanical Testing

Following μCT, all tibiae were monotonically tested to failure using four-point bending in displacement control at 0.025 mm/sec while fully hydrated. A loading span of 3 mm and support span of 9 mm were used (Figure 3.2). The tibia-fibula junction was placed just outside of the right-most loading point and oriented such that the bone was tested in the medial-lateral direction with the medial surface in tension. The distance from the proximal end of the bone to the location of fracture initiation was measured using calipers. Seven transverse slices were obtained from μCT images

at the location of fracture and the calculated geometric properties (bending moment of inertia and distance from the centroid to the extreme fiber in tension) were used to map load-displacement into stress-strain. Pre- and post-yield mechanical properties were obtained from the resulting curves, as previously described [37].

3.3.6 Statistics

The assumptions of normality and homoscedasticity were assessed and any violations were corrected using transformations. A repeated-measures ANOVA tested the main effects of loading (within-subject effect), strain level (between-subject effect), and their interaction ($\alpha = 0.05$). If strain level had a significant main effect in the absence of an interaction effect with loading, Tukeys HSD tests examined pairwise differences between strain levels ($\alpha = 0.025$) within loaded and non-loaded limbs separately. If an interaction was indicated, paired t-tests evaluated the effect of loading at each of the three strain levels (i.e. control limb versus loaded limb) and a one-way ANOVA evaluated the effect of strain level separately within the loaded and non-loaded limbs. After a Bonferroni correction, the significance level for the paired t-tests and one-way ANOVAs was set to $\alpha = 0.01$. If strain level had a significant effect from the ANOVA in either limb, post hoc pairwise differences were examined using Tukeys HSD tests in that limb ($\alpha = 0.01$). For the comparison of body mass between the start and end of loading, a repeated-measures ANOVA tested the main effects of age (day -1 vs. day 14) and strain level. Statistical tests were performed using SAS 9.4 (SAS Institute Inc., Cary, NC) and values are reported as the mean $\pm$ the standard deviation (SD).

3.4 Results

Following sacrifice, the tibiae were first scanned by μCT to analyze the structural adaptation of the bones. During the initial characterization of these scans, a woven cortical response was discovered in the loaded tibiae of five mice from the 2400 $\mu\epsilon$

group. The decision was made to remove both the loaded and non-loaded contralateral limbs from all future analyses (μCT and mechanical), reducing the sample size in each 2400 $\mu\epsilon$ group to n = 5. Data from the woven bone response have been included in the supplemental information, although no statistics were performed with those data included.

3.4.1 Animal Body Mass and Tibial Length

The body mass of each animal was recorded two days prior to the start of loading at Day -1 (1700 $\mu\epsilon$: 18.8 $\pm$ 1.0 g; 2050 $\mu\epsilon$: 18.8 $\pm$ 0.9 g; 2400 $\mu\epsilon$: 18.3 $\pm$ 1.1 g) and again on the final day of loading (1700 $\mu\epsilon$: 19.5 $\pm$ 1.2 g; 2050 $\mu\epsilon$: 19.2 $\pm$ 1.0 g; 2400 $\mu\epsilon$: 18.5 $\pm$ 1.3 g). Body mass and tibial lengths from animals with woven bone response were excluded. There was a significant increase in mass due to age (p<0.001), but no difference in body mass between groups. Tibial length was recorded at the end of the study. The length was compared between the control (1700 $\mu\epsilon$: 16.9 $\pm$ 0.6 mm; 2050 $\mu\epsilon$: 17.3 $\pm$ 0.4 mm; 2400 $\mu\epsilon$: 17.0 $\pm$ 0.3 mm) and loaded limbs (1700 $\mu\epsilon$: 16.9 $\pm$ 0.5 mm; 2050 $\mu\epsilon$: 17.2 $\pm$ 0.5 mm; 2400 $\mu\epsilon$: 17.0 $\pm$ 0.5 mm). There was no main effect of loading or strain level on tibial length.

3.4.2 Cortical and Cancellous Architecture

In a standard cancellous region of interest in the proximal metaphysis, all properties had main effects of loading, strain level, or interaction effects (Table 3.1). Trabecular thickness had a significant interaction effect (p = 0.038), and post hoc paired t-tests indicated that it was significantly higher in the loaded versus control limb at all three strain levels (p<0.001 in all cases). Trabecular thickness also increased as a function of strain level in the loaded limbs (p<001). Bone volume fraction (BV/TV) and TMD had significant main effects of strain level without a significant interactive effect (p = 0.027 and p = 0.002, respectively) indicating systemic effects of loading for these parameters, which were generally enhanced as strain increased. In addition to

the effect of strain level, there was also a significant main effect of loading in BV/TV and TMD (p = 0.013 and p<0.001, respectively) with both increasing in the loaded limb. There was a main effect of loading which increased trabecular separation (p = 0.012), decreased trabecular number (p = 0.001), and increased structural model index (p<0.001). These results suggest that loading caused fewer, thicker, and more rod-like trabeculae resulting in a greater bone volume in the metaphysis.

Table 3.1

Cancellous Architecture in the Proximal Metaphysis

	1700 $\mu\epsilon$		2050 $\mu\epsilon$		2400 $\mu\epsilon$	
	Control (n=10)	Loaded (n=10)	Control (n=10)	Loaded (n=10)	Control (n=5)	Loaded (n=5)
BV/TV (%)#,*	4.34 ± 1.14	4.66 ± 1.18	5.33 ± 0.86	5.30 ± 0.67	5.31 ± 0.80	6.33 ± 0.89[a]
Trabecular Thickness (μm)&	51.0 ± 1.5	58.7 ± 2.9[†]	52.1 ± 1.2	61.4 ± 2.3[†]	51.2 ± 1.3	66.0 ± 3.8[†,c]
Trabecular Number (1/mm)#	0.85 ± 0.22	0.79 ± 0.20	1.02 ± 0.18	0.86 ± 0.11	1.04 ± 0.17	0.97 ± 0.18
Trabecular Separation (mm)#	0.36 ± 0.04	0.37 ± 0.04	0.34 ± 0.03	0.35 ± 0.02	0.33 ± 0.03	0.35 ± 0.04
Structural Model Index#	2.44 ± 0.12	2.62 ± 0.18	2.37 ± 0.11	2.64 ± 0.11	2.37 ± 0.08	2.61 ± 0.14
Tissue Mineral Density (g/cm³)#,*	1.07 ± 0.03	1.13 ± 0.06	1.03 ± 0.03[a]	1.06 ± 0.02[a]	1.03 ± 0.03	1.06 ± 0.03[a]

Values are presented as mean ± standard deviation. In the property column, # indicates a main effect of loading and * indicates a main effect of strain level from repeated measures ANOVA (p<0.05) with no interactive effect. For the main effect of strain level in BV/TV and tissue mineral density, a One Way ANOVA with post hoc Tukeys HSD tests (when p<0.025) examined pairwise differences between strain levels within loaded and non-loaded limbs separately [a indicates a difference versus 1700 $\mu\epsilon$ (p<0.025)]. When there was a main interactive effect (indicated by & in the property column), a paired t-test evaluated the effect of loading at each strain level († indicates p<0.01 versus control) and a one-way ANOVA with post hoc Tukeys HSD tests (when p<0.01) evaluated differences between strain levels within loaded limbs [c indicates a difference versus 1700 $\mu\epsilon$ (p<0.01)].
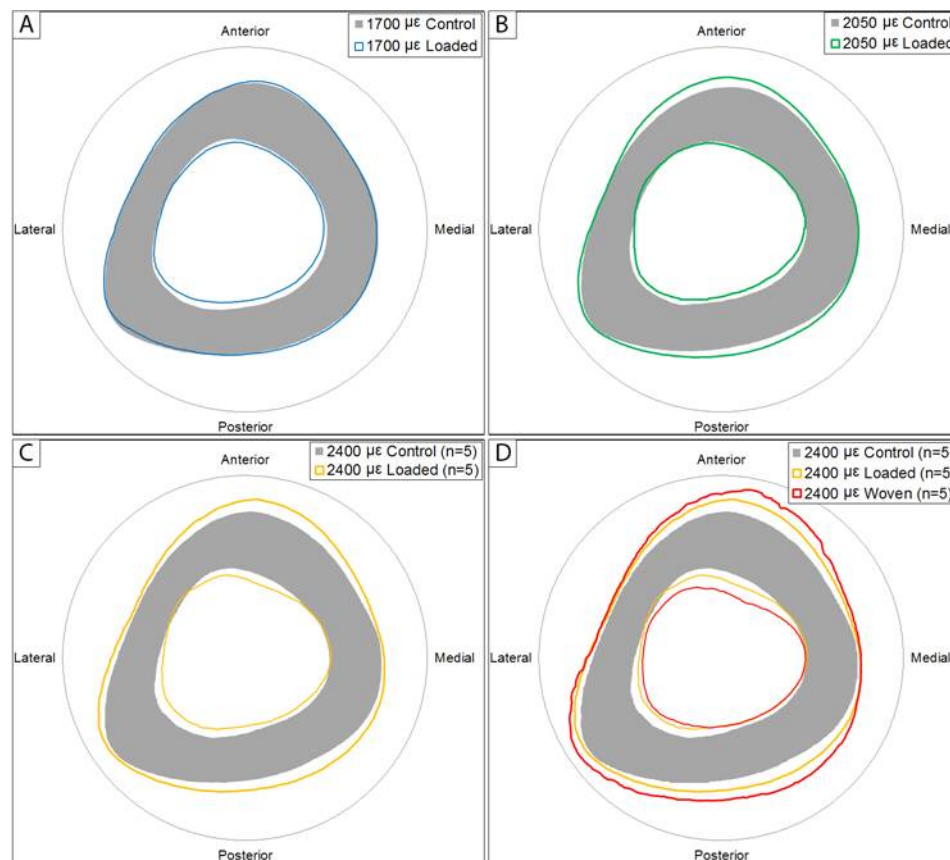
Fig. 3.3. Schematic Representations of Standard Site Geometric Profiles. A) 1700 $\mu\epsilon$ group. B) 2050 $\mu\epsilon$ group. C) 2400 $\mu\epsilon$ group. There was a dose-dependent increase in cortical parameters with robust periosteal and endocortical formation, especially at the higher strain levels. D) 2400 $\mu\epsilon$ group with the addition of those animals that experiences a woven bone response due to loading.

Cortical geometry was analyzed at a standard site within the mid-diaphysis of each bone (Table 3.2, Figure 3.3). Strain level only affected the loaded limbs and there were no main effects of strain level indicating no systemic effects at this site. Generally, loading increased the amount of bone present in a dose-dependent fashion. Total cross-sectional area was increased with loading versus control in the 2400 $\mu\epsilon$ group (p<0.001). Cortical area and thickness were greater in the loaded limb at all strain levels (p<0.001 at all levels) and this effect was more pronounced as strain increased. Loading reduced marrow area and endocortical perimeter (main effect of loading,

both p<0.001) indicating endocortical contraction. Loading increased maximum and minimum principal moments of inertia and, taking the increasing trend in periosteal perimeter into consideration (significant at 2400 $\mu\epsilon$, p<0.001), these results indicate periosteal expansion accompanies the endocortical contraction. Periosteal expansion occurred primarily in the anterior-posterior (AP) direction as seen by significant increases in AP width as a function of strain in the loaded limb and the significant increase in loaded versus control limbs at 2050 $\mu\epsilon$ (p = 0.002), Medial-lateral (ML) width was unaffected by loading or strain level, as was cortical TMD.

Table 3.2: Cortical Geometry at the Mid-Diaphysis

	1700 $\mu\epsilon$		2050 $\mu\epsilon$		2400 $\mu\epsilon$	
	Control (n=10)	**Loaded (n=10)**	**Control (n=10)**	**Loaded (n=10)**	**Control (n=5)**	**Loaded (n=5)**
Cross Sectional Area (mm²)&	0.836 ± 0.070	0.836 ± 0.050	0.827 ± 0.051	0.877 ± 0.033	0.833 ± 0.057	0.924 ± 0.019[†,d]
Cortical Area (mm²)&	0.494 ± 0.042	0.524 ± 0.028[†]	0.496 ± 0.032	0.568 ± 0.027[†,c]	0.501 ± 0.036	0.628 ± 0.012[†,c,d]
Marrow Area (mm²)#	0.342 ± 0.033	0.311 ± 0.029	0.331 ± 0.023	0.310 ± 0.029	0.332 ± 0.026	0.296 ± 0.010
Cortical Thickness (mm)&	0.186 ± 0.009	0.201 ± 0.007[†]	0.188 ± 0.007	0.215 ± 0.012[†,c]	0.189 ± 0.008	0.235 ± 0.004[†,c,d]
AP Width (mm)&	1.050 ± 0.054	1.057 ± 0.030	1.016 ± 0.031	1.079 ± 0.024[†]	1.044 ± 0.052	1.127 ± 0.029[c]
ML Width (mm)	1.055 ± 0.050	1.053 ± 0.050	1.070 ± 0.056	1.080 ± 0.032	1.067 ± 0.038	1.104 ± 0.038
Periosteal Perimeter (mm)&	3.885 ± 0.165	3.898 ± 0.113	3.858 ± 0.126	3.981 ± 0.070	3.888 ± 0.137	4.102 ± 0.046[†,d]
Endocortical Perimeter (mm)#	2.552 ± 0.122	2.449 ± 0.122	2.515 ± 0.094	2.431 ± 0.117	2.533 ± 0.102	2.401 ± 0.024

Table 3.2: (continued)

	1700 $\mu\epsilon$		2050 $\mu\epsilon$		2400 $\mu\epsilon$	
	Control (n=10)	**Loaded** (n=10)	**Control** (n=10)	**Loaded** (n=10)	**Control** (n=5)	**Loaded** (n=5)
I_{max} (mm^4)$^{\&}$	0.055 ± 0.011	0.055 ± 0.008	0.054 ± 0.008	0.063 ± 0.006†	0.055 ± 0.009	0.072 ± 0.004^c
I_{min} (mm^4)$^{\&}$	0.041 ± 0.006	0.043 ± 0.004	0.040 ± 0.004	0.047 ± 0.003†	0.041 ± 0.005	0.053 ± 0.003^{†,c}
Tissue Mineral Density (g/cm^3)	1.316 ± 0.023	1.328 ± 0.022	1.316 ± 0.021	1.318 ± 0.020	1.314 ± 0.024	1.301 ± 0.034

Values are presented as mean ± standard deviation. In the property column, # indicates a main effect of loading with no interactive effect. When there was a main interactive effect (indicated by & in the property column), a paired t-test evaluated the effect of loading at each strain level († indicates p<0.01 versus control) and a one-way ANOVA with post hoc Tukeys HSD tests (when p<0.01) evaluated differences between strain levels within loaded limbs [c indicates a difference versus loaded limbs [c indicates a difference versus 1700 $\mu\epsilon$ (p<0.01) and 'd' indicates a difference verses 2050 $\mu\epsilon$ (p<0.01)].

3.4.3 Mechanical Properties from Four-Point Bending

Four-point bending was used to investigate changes in mechanical properties due to in vivo loading. Structural and tissue-level mechanical properties are shown in Table 3.3 and 3.4, respectively. In addition, schematic representations of mechanical data are shown in Figure 3.4. These schematic curves were generated by averaging data from the yield point, the point of maximum force/stress and the failure point across all samples within a group. Although they were not statistically analyzed in this form, the curves make a qualitative comparison between groups easier. As noted above, loaded and contralateral limbs from animals experiencing a woven bone response at the highest strain level were excluded from statistical analysis (data are shown in the supplemental information for the purpose of qualitative comparison). Excluding these bones dropped the sample size from n = 10 to n = 5 for the 2400 $\mu\epsilon$ group. In addition, the control group at that strain level had an excluded statistical outlier which, in the paired post hoc analyses, resulted in n = 4 for both the control and loaded groups.

Table 3.3: Structural Mechanical Properties From 4-Point Bending of the Mid- Diaphysis

	1700 $\mu\epsilon$		2050 $\mu\epsilon$		2400 $\mu\epsilon$	
	Control (n=9)	Loaded (n=9)	Control (n=9)	Loaded (n=9)	Control (n=4)	Loaded (n=5)
Yield Force(N)[&]	12.47 ± 1.47	12.47 ± 1.46	10.88 ± 2.39	14.22 ± 2.48[‡]	11.05 ± 1.31	12.06 ± 1.73
Ultimate Force (N)[&]	13.86 ± 1.39	13.36 ± 1.48	13.11 ± 2.11	18.21 ± 2.50[†,c]	15.16 ± 2.60	18.54 ± 1.37[c]
Stiffness (N/mm)[*]	67.30 ± 13.05	70.80 ± 19.93	76.81 ± 16.53	93.06 ± 12.60[a]	87.92 ± 8.76	92.25 ± 9.82
Deformation to Yield (μm)[*]	214 ± 33	214 ± 51	174 ± 45	184 ± 42	154 ± 17	155 ± 18
Postyield Displacement (μm)	538 ± 292	401 ± 307	476 ± 174	727 ± 301	558 ± 226	755 ± 275
Total Deformation (μm)	752 ± 291	615 ± 286	650 ± 184	911 ± 326	712 ± 226	910 ± 259

Table 3.3: (continued)

	1700 $\mu\epsilon$		2050 $\mu\epsilon$		2400 $\mu\epsilon$	
	Control (n=9)	**Loaded** (n=9)	**Control** (n=9)	**Loaded** (n=9)	**Control** (n=4)	**Loaded** (n=5)
Work to Yield (mJ)	1.45 ± 0.33	1.48 ± 0.38	1.06 ± 0.47	1.50 ± 0.58	0.96 ± 0.23	1.07 ± 0.26
Postyield Work (mJ)&	5.81 ± 3.33	4.34 ± 3.30	4.96 ± 2.15	11.09 ± 4.29[†,c]	7.06 ± 2.72	11.95 ± 3.90[c]
Work to Failure (mJ)&	7.26 ± 3.35	5.82 ± 3.20	6.02 ± 2.26	12.59 ± 4.60[†,c]	8.02 ± 2.76	13.01 ± 3.67[c]

Values are presented as mean ± standard deviation. In the property column, * indicates a main effect of strain level from repeated measures ANOVA ($p<0.05$) with no interactive effect. When there was a main effect of strain level, a One Way ANOVA with post hoc Tukeys HSD tests (when $p<0.025$) examined pairwise differences between strain levels within loaded and non-loaded limbs separately [a indicates a difference versus 1700 $\mu\epsilon$ ($p<0.025$)]. When there was a main interactive effect (indicated by & in the property column), a paired t-test evaluated the effect of loading at each of the strain levels († indicates $p<0.01$ versus control) and a one-way ANOVA with post hoc Tukeys HSD tests (when $p<0.01$ which only occurred in loaded limbs) evaluated differences between strain levels within loaded limbs [c indicates a difference versus 1700 $\mu\epsilon$ ($p<0.01$)]. For 2050 $\mu\epsilon$, a marginal difference between loaded and control limbs for yield force ($p = 0.02$) is noted with ‡.

No structural or tissue-level mechanical properties in the 1700 $\mu\epsilon$ or 2400 $\mu\epsilon$ groups had a significant change with loading, but there were several significant differences within the 2050 $\mu\epsilon$ group. At 2050 $\mu\epsilon$, loading significantly increased ultimate force (p<0.001), postyield work (p = 0.010), and work to failure (p = 0.010). There was also a trend towards increased yield force due to loading (p = 0.020). For estimated tissue-level properties, ultimate stress was significantly increased with loading in the 2050 $\mu\epsilon$ group (p = 0.007). In addition, although not significant given the stringent statistical threshold, toughness was marginally increased with loading (p = 0.012). Overall, the data indicate loading results in stronger tissue and structure which dissipates more energy prior to failure for the 2050 $\mu\epsilon$ group. Stiffness, deformation to yield, and strain to yield all exhibited systemic effects due to loading as indicated by the significant main effect of strain level (p = 0.007, p = 0.012, and p = 0.017, respectively). Strain to failure also had a significant main effect of strain (p = 0.050), but this effect was dominated by effects in the loaded limb.

Table 3.4: Estimated Tissue-Level Mechanical Properties from 4-Point Bending of the Mid-Diaphysis

	1700 $\mu\epsilon$		2050 $\mu\epsilon$		2400 $\mu\epsilon$	
	Control (n=9)	Loaded (n=9)	Control (n=9)	Loaded (n=9)	Control (n=4)	Loaded (n=5)
Yield Stress (MPa)	188.9 ± 35.4	186.8 ± 34.6	169.3 ± 56.0	212.6 ± 53.0	157.8 ± 33.7	147.5 ± 55.5
Ultimate Stress (MPa)$^{\&}$	210.5 ± 40.7	200.1 ± 34.5	204.7 ± 59.0	267.5 ± 34.3[†]	212.3 ± 22.3	224.3 ± 79.2
Elastic Modulus (MPa)	13.83 ± 5.17	14.86 ± 5.27	15.61 ± 6.05	18.93 ± 3.96	16.69 ± 7.54	14.56 ± 7.14
Strain to Yield ($\mu\epsilon$)[*]	16230 ± 2626	15221 ± 3724	13346 ± 2840	13414 ± 2756	12355 ± 2312	12607 ± 1355

Table 3.4: (continued)

	1700 $\mu\epsilon$		2050 $\mu\epsilon$		2400 $\mu\epsilon$	
	Control (n=9)	**Loaded** (n=9)	**Control** (n=9)	**Loaded** (n=9)	**Control** (n=4)	**Loaded** (n=5)
Strain to Failure ($\mu\epsilon$)[*]	56337 ± 19632	43864 ± 19630	49855 ± 12397	66456 ± 23364	57453 ± 20519	78167 ± 36418
Resilience (MPa)	1.64 ± 0.33	1.58 ± 0.45	1.26 ± 0.59	1.64 ± 0.68	1.07 ± 0.19	1.02 ± 0.32
Toughness (MPa)[&]	8.32 ± 3.82	6.25 ± 3.69	7.11 ± 2.74	13.66 ± 5.29[‡,c]	8.87 ± 2.81	12.00 ± 2.20

Values are presented as mean ± standard deviation. In the property column, * indicates a main effect of strain from repeated measures ANOVA (p<0.05) with no interactive effect. When there was a main effect of strain level, a separate One Way ANOVA on strain levels within loaded and non-loaded limbs failed to reach significance for any property. When there was a main interactive effect (indicated by & in the property column), a paired t-test evaluated the effect of loading at each of the strain levels († indicates p<0.01 versus control) and a one-way ANOVA with post hoc Tukeys HSD tests (when p<0.01 which only occurred in loaded limbs) evaluated differences between strain levels within loaded limbs [c indicates a difference versus 1700 $\mu\epsilon$ (p<0.01)]. For 2050 $\mu\epsilon$, a marginal difference between loaded and control limbs for toughness (p = 0.0123) is noted with ‡.

3.5   Discussion

Over the past 10 years, axial loading of the tibia has become a well-accepted and heavily utilized bone adaptation model. Despite this fact, few studies have explored the mechanical impacts of targeted tibial loading [18,22,28], and instead have focused on morphological changes. While investigating an adaptive formation response and changes in bone architecture are important, failure to modify mechanical properties may lessen the broader impact of loading or the potential to use the model to enhance properties of diseased bone. The goal here was to investigate how mechanical properties change in response to targeted tibial loading while also exploring changes in cortical and trabecular architecture. We hypothesized that loading would lead to dose-dependent increases in cortical and trabecular architecture while also increasing bone- and tissue-level stiffness, strength, and ductility. In general, the data confirmed our hypothesis of a dose-dependent response of strain level improving cortical and cancellous architecture and increasing mechanical properties, but changes in mechanical properties could not be explained by a simple linear dose-dependent model. The different relationships between morphological and mechanical properties highlight the importance of assessing mechanics along with morphology in future loading studies. Half of the mice loaded to 2400 $\mu\epsilon$ experienced a woven bone response. As discussed below, other factors indicated that loading to 2400 $\mu\epsilon$ in future studies should be avoided.

This study is not the first to investigate the strain-specific response to loading [30–33]. However, because the age and loading parameters in the various studies differ, there is no way to directly compare the responses. In addition, mechanical outcomes were rarely assessed. One study using female B6 mice at the same starting age as in our study (8 weeks) subjected the animals to load levels ranging from 5-13 N [31], but calibrated strain values were only reported for 12 week old mice so it is not clear what strain level these loads equated to at 8 weeks. In that study, loading tended to increase trabecular and cortical parameters at all ages with greater

responses at higher load levels. A similar positive response to loading was reported for female B6 mice loaded between 0 and 14 N [32], but this group also reported a woven response in cortical bone at 14 N, similar to what was seen at 12.4 N in the current study. A third study loaded 26 week old female B6 mice to 5.9 N (1200 $\mu\epsilon$) or 11.3 N (2100 $\mu\epsilon$) for 2 weeks [30]. In that case, adaptation only occurred at the higher strain level where cancellous bone mass (via increased trabecular thickness) and cortical area (via periosteal and endocortical apposition) both increased. As with this previous work, a dose-dependent change in response to loading was noted in the current study for trabecular and cortical morphological parameters.

Improvements in trabecular architecture were driven by increases in trabecular thickness but at the cost of reducing trabecular number (Table 3.1). The reduction in trabecular number accounts for bone volume fraction only being significantly improved in the high strain group of the loaded limbs despite gains in thickness at all strain levels. Because the proximal metaphysis of this age and strain of mice is sparsely filled with trabeculae and continually declines with age starting at 8 weeks [38, 39], small changes in the total number of trabecular struts could produce the significant decrease noted here. However, the decrease in the number of trabeculae may be an artifact of adjacent trabeculae thickening in the loaded limb to the point of closing their gap below the resolution of the μCT (approximately 10 m) and being tallied as one trabecular strut.

Trabecular tissue mineral density was significantly decreased as a function of strain level in both loaded and non-loaded limbs suggesting that there are systemic effects from in vivo loading in the contralateral limb (Table 3.1). Loading did not induce an osteogenic response in the contralateral limb, so while decreases in tissue mineralization could be explained by decreased tissue age in the loaded limb, this would not explain decreased mineral density in the contralateral limb. A previous study employing an additional caged control group did not detect systemic effects in volumetric bone mineral density (vBMD) [22], but direct comparisons between tissue mineral density and vBMD are difficult because vBMD superimposes changes in tis-

sue mineral density onto changes in BV/TV. As in previous studies [22, 40], neither cancellous nor cortical architecture displayed any systemic effects. However, in the present study, both structural- and tissue-level mechanical properties were altered in the non-loaded limb as a function of strain level, particularly in the pre-yield region, indicating systemic effects. Loading to increasing strain levels systemically increased stiffness (approximately 30% for non-loaded and loaded limbs from 1700 $\mu\epsilon$ to 2400 $\mu\epsilon$) causing bones to reach yield at lower displacements (Table 3.3) and strains (Table 3.4). While the main effect of strain level on elastic modulus did not reach significance, there was a general trend for increased elastic modulus at increasing strains, especially in the non-loaded limbs. A previous study showed no systemic changes in stiffness [22], but differences between these studies may be explained by age (22 weeks vs 10 weeks at sacrifice), duration of loading (6 weeks vs 2 weeks), mechanical testing modality (axial compression vs four-point bending), or strain level (compressive posterolateral 2800 $\mu\epsilon$ vs tensile anteromedial 2050 $\mu\epsilon$) which, in the previous report, was high enough to damage existing tissue resulting in reduced stiffness. The implications that loading could improve the mechanical integrity of existing tissue in the contralateral limb are intriguing, and these systemic effects should be considered in future studies investigating mechanical properties or mineralization.

The current study is also not the first to characterize mechanical implications following tibial loading [18, 22, 28]. Only one previous study performed a full mechanical characterization following loading, but only reported structural properties by testing bones to failure in axial compression [22]. Given that the in vivo loading model is performed in axial compression, assessing ex vivo mechanical properties in this configuration is ideal since one would expect the adaptive response (if any) to be strongest in that orientation. In a pilot study, we attempted to load bones to failure in this manner but most failed at the epiphysis rather than in the diaphysis due to the compressive/bending loads induced in the bone. It is possible that because the animals used in the previous study were skeletally mature [22] versus the growing mice used here, the epiphyses were closed (or more fully mineralized) and therefore more

structurally sound. Loading generally increased deformation and energy dissipation when bones were loaded to failure in axial compression [22]. In the current study, structural- and tissue-level energy dissipation were also increased, and although total deformation and strain to failure trended up, they failed to reach significance in any group. The current study also demonstrated increased ultimate force and ultimate stress with loading (Tables 3.3 and 3.4, Figure 3.4). These significant mechanical changes came specifically in the mid strain (2050 $\mu\epsilon$) group. The lowest strain level (1700 of tension) had little effect on structural and tissue-level strength and energy dissipation. The highest strain group (2400 $\mu\epsilon$ of tension) showed little to no increases in strength and energy dissipation versus those realized in the 2050 $\mu\epsilon$ group. Loadings effect size (loaded versus control) at 2400 $\mu\epsilon$ was reduced due to values in the non-loaded limb trending toward the loaded values compared to the effect at 2050 $\mu\epsilon$. Therefore, the lower sample sizes, only modest gains or losses in the loaded limbs, and baseline drift in the non-loaded limbs all contributed to the effect of loading at 2400 $\mu\epsilon$ not reaching significance.

Half of the animals loaded to 2400 $\mu\epsilon$ experienced a robust woven bone response, suggesting a potentially pathological response to loading (Supplemental Figures 3.5-3.7, Table 3.5). It is important to note that many of the mice in this high strain group demonstrated a slight limping after recovering from anesthesia immediately following loading. The limp was short lived, but suggests that the loading itself may have been painful as previously shown when loading to 13 N [31]. When harvesting tissues, it was clear that some of the tibiae from the high strain group had bumpy nodules near the proximal end of the bone. When the woven response was discovered in five of these animals upon analysis of cortical μCT data, the decision was made to remove those animals from all analyses (both the loaded and its contralateral limb). The contralateral limb was removed as there was a concern of a potentially biasing a systemic response to loading. The data from the removed animals appear in the supplemental information for comparison but was not included in any statistical analyses. It is clear both from the mechanical data and to a lesser degree from the

cortical and trabecular analysis that a woven response on the loaded side did in fact alter the non-loaded control limbs. While we believe this was the proper way to handle the data, the drawback of this decision was a loss of power [e.g. TMD is decreased by the same amount in the control limb from both the 2050 $\mu\epsilon$ and 2400 $\mu\epsilon$ groups versus the 1700 $\mu\epsilon$ group but only reached significance in the 2050 group (Table 3.1)]. Our sample size started at n = 10 but the woven response dropped this to n = 5. The sample size was further reduced for the mechanical characterizations due to mechanical testing anomalies (one mechanical sample was lost from each group except the loaded bones of the 2400 $\mu\epsilon$ group). Because of the paired nature of the post hoc comparisons, this further reduces the sample size for the comparison of loaded versus control limbs (n = 8 for 1700 $\mu\epsilon$ and 2050 $\mu\epsilon$; n = 4 for 2400 $\mu\epsilon$). Although the starting sample size was sufficient for mechanical studies, losing samples and the associated lost power reduced our ability to detect differences in some groups. Therefore, despite what appear to be morphological and mechanical benefits, the combination of pain, a woven cortical response, and potential pathological nodule formation suggests that loading above the 2050 $\mu\epsilon$ level is unnecessary and should be avoided.
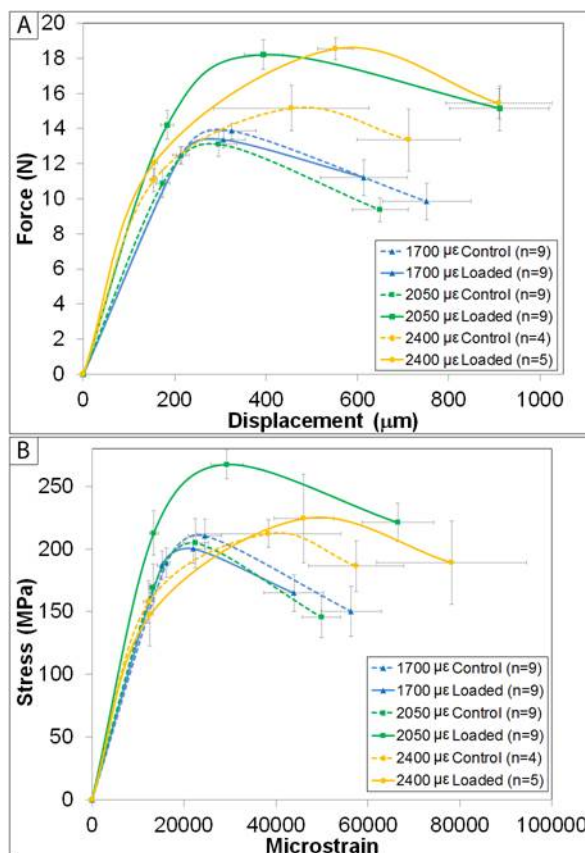
Fig. 3.4. Schematic representations of mechanical testing curves. A) Representative structural-level force/displacement curves. B) Estimated tissue-level mechanical curves. At 1700 $\mu\epsilon$, there was no mechanical effect noted. Those limbs loaded to 2050 $\mu\epsilon$ experienced significant increases in structural- and tissue-level strength and energy dissipation. The 2400 $\mu\epsilon$ group also experienced gains. However, when animals that experienced a woven bone response were removed from the analysis, the gains were more modest (especially at the tissue-level) and most failed to reach significance versus the contralateral control limb given the loss in power. For all data points, error bars represent the standard error of the mean (SEM).

When performing in vivo loading studies in individual limbs, the importance of proper calibration cannot be overlooked. Some published papers lack the details of their experiments [41]. A more widespread issue is that many papers do not perform a new calibration and, instead, use data from previously published papers for the same inbred strain, age, and sex [12,17,40,42]. This approach can be problematic, as

exemplified by the following example. In some papers, the authors only publish the slope of the calibration curve (often called the stiffness and reported as the inverse of the slope, in $N/\mu\epsilon$). However, the actual calibration curve is linear, meaning it has a slope and a y-intercept. If strain were on the y-axis, the intercept would be the non-zero strain at zero load. Few papers show this intercept value but it has been reported to be as high as 454 $\mu\epsilon$ [13, 20, 33]. On its own, disregarding this component of the strain calibration could alter the force necessary to attain the desired strain level.

As part of ongoing studies in our laboratory, two other strain calibrations have been performed. Animals used in all strain gauging studies were purchased from the same vendor (Harlan Laboratories, Indianapolis IN). All were female mice from the C57BL/6NHsd inbred strain, and all arrived at our facility at 7 weeks of age and were allowed 1 full week of acclimation prior to the initiation of the studies. The only difference between the mice was that they came from different animal lots, being purchased individually for each experiment at three times over a roughly 12 month period. For each study, the strain gauge application and calibration procedures were identical and performed by the same operator. Surprisingly, results obtained from the three studies were not the same. All three experiments produced linear force/strain relationships (Supplemental Figure 3.7). However, data from the second experiment differed from those obtained in experiments 1 and 3. This difference in calibration could lead to incorrect strain values if used improperly. As an example, the highest strain group in the current study was loaded to 12.4 N for a target strain of 2400 $\mu\epsilon$. This same 12.4 N would have generated approximately 2300 $\mu\epsilon$ using the calibration and mice from experiment #1, likely within the error of the calibration curve and loading device. However, 12.4 N would have generated 3150 $\mu\epsilon$ in experiment #2.

Recalling that the only difference between the experiments was the lot of mice used begs the question: why do mice from the same age, gender, and inbred strain from the same vendor produce different calibration curves? The answer is not straightforward, but may partially be driven by slight differences in animal body mass. According

to growth curves provided by Harlan [43], 8 week old female B6 mice should weigh approximately 17.9 g. The mice from the three lots used in this study were all greater than this. For study #1 and #3, the average mass was 18.8 ± 1.3 g and 18.8 ± 0.9 g, respectively. However, the mass from study #2 was 19.4 ± 0.9 g and although it was within the mean ± 2 SDs, may have caused the noted effect on the calibration. Looking through the tibial loading literature, only one paper began loading female B6 mice at 8 weeks but did not include body mass data [31]. However, several started loading just before or just after this age. In 2005, Fritton used B6 females from Jackson Labs [29]. At 7 weeks of age, those mice weighed 21.4 g, considerably higher than our 8 week mass. A 2013 study using 10 week old B6 females had a mass of 16.9 g, lower than our 8 week mass [23]. In 2014, Main et al. 10 week B6 females with a mass of 18.6 g, similar to 2 of our groups at 8 weeks [10]. In the end, it is not possible to determine if this difference in mass is responsible for the variation in calibration. However, it highlights the importance of performing a new set of calibrations at the start of every loading study on weight-matched mice from the same lot used for the actual loading study and as close to the start of loading as possible.

In conclusion, the current study demonstrated the expected positive impact of direct loading on cortical and cancellous architecture while also indicating that this form of loading, even in a short-term model, can lead to significant increases in structural- and tissue-level mechanical behavior. This focus on mechanical end points is lacking in the literature but is important if the loading regimen is to used be for functional gain (e.g. to enhance properties of diseased bone). A woven cortical response initiated at the highest load level (12.4 N, 2400 $\mu\epsilon$) resulted in robust tissue formation and mechanical gains, but came at the cost of animal discomfort and a potential systemic response in the contralateral limb. Future studies utilizing this model should focus on a more moderate load level which was largely beneficial in young female mice both in terms of cortical/cancellous structure and mechanical function.

3.6 Funding Sources

3.7 Conflict of Interest

We wish to confirm that there are no known conflicts of interest associated with this publication and there has been no financial support for this work that could have influenced its outcome.

3.8 Supplemental
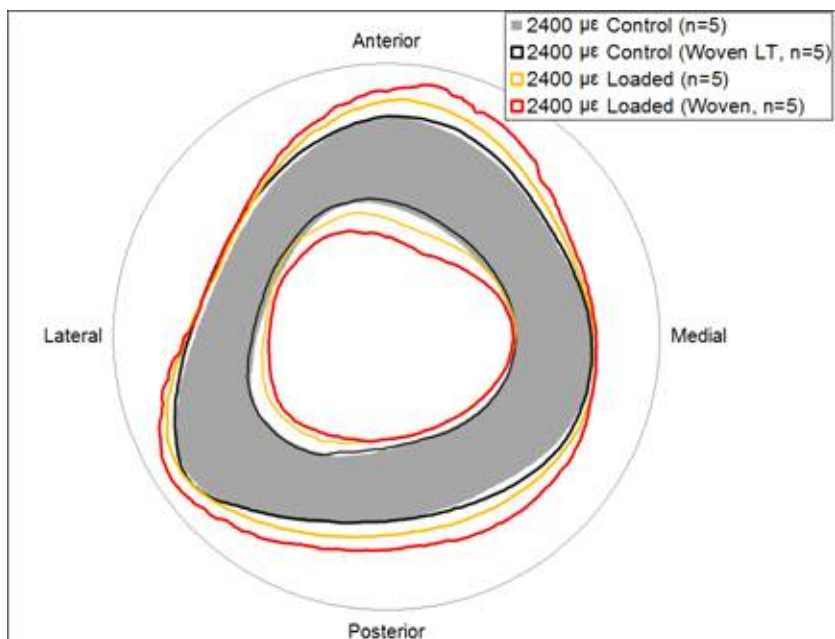
Fig. 3.5. Schematic representations of Standard Site Geometric Profiles from the 2400 $\mu\epsilon$ group. There is a potential systemic response when woven bone formation was initiated due to loading. The shaded bone in the background is from the control limb of animals with a normal formation response on the loaded contralateral side (solid yellow profile). When animals experienced a woven bone response due to loading (outermost periosteal and innermost endocortical profiles in red), the contralateral non-loaded limb (black) also appears to have experienced a primarily periosteal response. As a point of comparison, the periosteal perimeter of the non-loaded limb of animals experiencing a woven response increased by 0.78% versus the non-loaded limb of animals without a woven response. In the 1700 $\mu\epsilon$ group, the effect of loading was to increase the total cross sectional area by 0.34%.
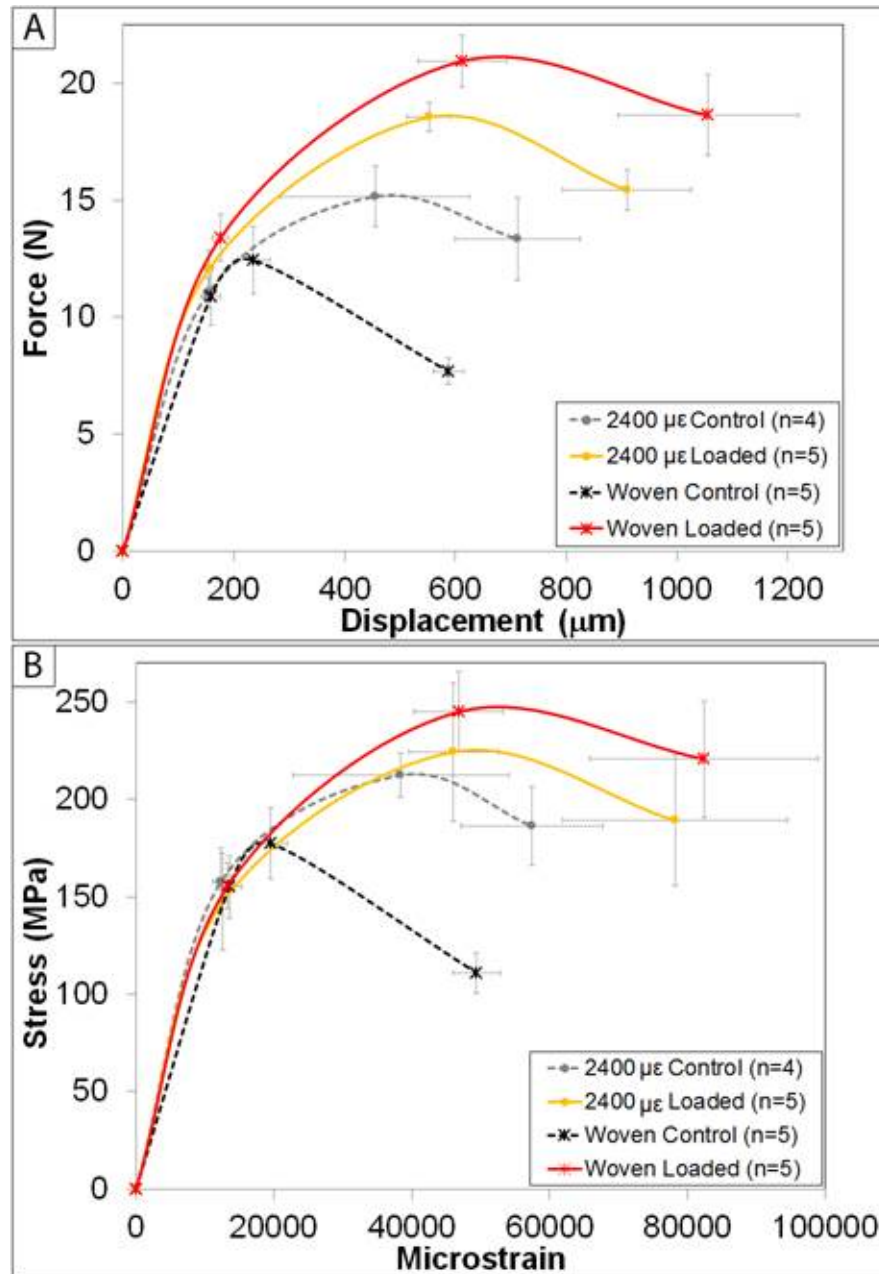
Fig. 3.6. Schematic representations of mechanical testing curves from the 2400 $\mu\epsilon$ group. This figure shows the systemic response when woven bone formation was initiated due to loading. The contralateral limb from animals which experienced a cortical woven bone response (black, lowest curve in each panel) had decreased strength and stiffness relative to the control limb from animals with no woven response (grey dashed curve). For all data points, error bars represent the standard error of the mean (SEM).

Fig. 3.7. Calibration Curves from the current study and two previous pilot studies. This figure demonstrates the difference in calibration between three different studies performed. For all data points, error bars represent the standard deviation.

Table 3.5

Proximal Tibia Cancellous Architecture from the 2400 $\mu\epsilon$ Group

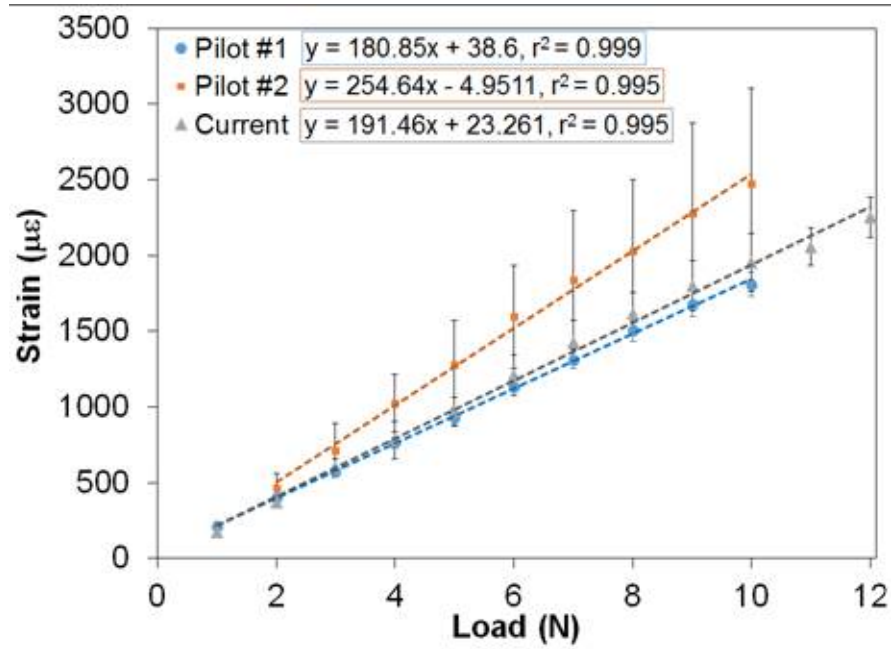|	Control (n=5)	Loaded (n=5)	Control from Woven Response (n=5)	Woven Response (n=5)
BV/TV (%)	5.31 ± 0.80	6.33 ± 0.89	5.22 ± 0.93	6.39 ± 0.82
Trabecular Thickness (μm)	51.2 ± 1.3	66.0 ± 3.8	51.7 ± 1.7	72.6 ± 4.4
Trabecular Number (1/mm)	1.04 ± 0.17	0.97 ± 0.18	1.01 ± 0.16	0.88 ± 0.07
Trabecular Separation (mm)	0.33 ± 0.03	0.34 ± 0.04	0.35 ± 0.02	0.37 ± 0.03
Structural Model Index	2.37 ± 0.08	2.61 ± 0.14	2.33 ± 0.11	2.65 ± 0.05
Tissue Mineral Density (g/cm^3)	1.03 ± 0.03	1.06 ± 0.03	1.05 ± 0.01	1.07 ± 0.02

Values are presented as mean $\pm$ standard deviation. As opposed to the cortical and mechanical systemic response due to woven bone formation, the changes in cancellous bone were less pronounced.

3.9 References

[1] J.-Y. Rho, L. Kuhn-Spearing, and P. Zioupos, "Mechanical properties and the hierarchical structure of bone," *Medical Engineering and Physics*, vol. 20, no. 2, pp. 92–102, 1998.

[2] P. Kannus, H. Sievnen, T. L. N. Jrvinen, M. Jrvinen, M. Kvist, P. Oja, I. Vuori, and L. Jozsa, "Effects of free mobilization and low- to high-intensity treadmill running on the immobilization-induced bone loss in rats," *Journal of Bone and Mineral Research*, vol. 9, no. 10, pp. 1613–1619, 1994.

[3] Y. Kodama, Y. Umemura, S. Nagasawa, W. G. Beamer, L. R. Donahue, C. R. Rosen, D. J. Baylink, and J. R. Farley, "Exercise and mechanical loading increase periosteal bone formation and whole bone strength in c57bl/6j mice but not in c3h/hej mice," *Calcified Tissue International*, vol. 66, no. 4, pp. 298–306, 2000.

[4] J. Mathey, M. N. Horcajada-Molteni, B. Chanteranne, C. Picherit, C. Puel, P. Lebecque, C. Cubizoles, M. J. Davicco, V. Coxam, and J. P. Barlet, "Bone mass in obese diabetic zucker rats: Influence of treadmill running," *Calcified Tissue International*, vol. 70, no. 4, pp. 305–311, 2002.

[5] A. Swissa-Sivan, A. Simkin, I. Leichter, A. Nyska, M. Nyska, M. Statter, A. Bivas, J. Menczel, and S. Samueloff, "Effect of swimming on bone growth and development in young rats," *Bone and Mineral*, vol. 7, no. 2, pp. 91–105, 1989.

[6] S. E. Warner, J. E. Shea, S. C. Miller, and J. M. Shaw, "Adaptations in cortical and trabecular bone in response to mechanical loading with and without weight bearing," *Calcified Tissue International*, vol. 79, no. 6, pp. 395–403, 2006.

[7] K. C. L. Lee, A. Maxwell, and L. E. Lanyon, "Validation of a technique for studying functional adaptation of the mouse ulna in response to mechanical loading," *Bone*, vol. 31, no. 3, pp. 407–412, 2002.

[8] K. Lee, H. Jessop, R. Suswillo, G. Zaman, and L. Lanyon, "The adaptive response of bone to mechanical loading in female transgenic mice is deficient in the absence of oestrogen receptor-alpha and -beta," *Journal of Endocrinology*, vol. 182, no. 2, pp. 193–201, 2004.

[9] M. D. Martinez, G. J. Schmid, J. A. McKenzie, D. M. Ornitz, and M. J. Silva, "Healing of non-displaced fractures produced by fatigue loading of the mouse ulna," *Bone*, vol. 46, no. 6, pp. 1604–12, 2010.

[10] R. P. Main, M. E. Lynch, and M. C. van der Meulen, "Load-induced changes in bone stiffness and cancellous and cortical bone mass following tibial compression diminish with age in female mice," *J Exp Biol*, vol. 217, no. Pt 10, pp. 1775–83, 2014.

[11] R. P. Main, M. E. Lynch, and M. C. H. van der Meulen, "In vivo tibial stiffness is maintained by whole bone morphology and cross-sectional geometry in growing female mice," *Journal of Biomechanics*, vol. 43, no. 14, pp. 2689–2694, 2010.

[12] N. Holguin, M. D. Brodt, M. E. Sanchez, and M. J. Silva, "Aging diminishes lamellar and woven bone formation induced by tibial compression in adult c57bl/6," *Bone*, vol. 65, pp. 83–91, 2014.

[13] T. K. Patel, M. D. Brodt, and M. J. Silva, "Experimental and finite element analysis of strains induced by axial tibial compression in young-adult and old female c57bl/6 mice," *J Biomech*, vol. 47, no. 2, pp. 451–7, 2014.

[14] M. D. Brodt and M. J. Silva, "Aged mice have enhanced endocortical response and normal periosteal response compared with young-adult mice following 1 week of axial tibial compression," *J Bone Miner Res*, vol. 25, no. 9, pp. 2006–15, 2010.

[15] M. J. Silva, M. D. Brodt, M. A. Lynch, A. L. Stephens, D. J. Wood, and R. Civitelli, "Tibial loading increases osteogenic gene expression and cortical bone volume in mature and middle-aged mice," *PLoS ONE*, vol. 7, no. 4, p. e34980, 2012.

[16] B. M. Willie, A. I. Birkhold, H. Razi, T. Thiele, M. Aido, B. Kruck, A. Schill, S. Checa, R. P. Main, and G. N. Duda, "Diminished response to in vivo mechanical loading in trabecular and not cortical bone in adulthood of female c57bl/6 mice coincides with a reduction in deformation to load," *Bone*, vol. 55, no. 2, pp. 335–346, 2013.

[17] A. I. Birkhold, H. Razi, G. N. Duda, R. Weinkamer, S. Checa, and B. M. Willie, "Mineralizing surface is the main target of mechanical stimulation independent of age: 3d dynamic in vivo morphometry," *Bone*, vol. 66, pp. 15–25, 2014.

[18] H. Razi, A. I. Birkhold, P. Zaslansky, R. Weinkamer, G. N. Duda, B. M. Willie, and S. Checa, "Skeletal maturity leads to a reduction in the strain magnitudes induced within the bone: A murine tibia study," *Acta Biomaterialia*, vol. 13, no. 0, pp. 301–310, 2015.

[19] M. E. Lynch, R. P. Main, Q. Xu, D. J. Walsh, M. B. Schaffler, T. M. Wright, and M. C. van der Meulen, "Cancellous bone adaptation to tibial compression is not sex dependent in growing mice," *J Appl Physiol (1985)*, vol. 109, no. 3, pp. 685–91, 2010.

[20] L. B. Meakin, G. L. Galea, T. Sugiyama, L. E. Lanyon, and J. S. Price, "Age-related impairment of bones' adaptive response to loading in mice is associated with sex-related deficiencies in osteoblasts but no change in osteocytes," *J Bone Miner Res*, vol. 29, no. 8, pp. 1859–71, 2014.

[21] L. B. Meakin, T. Sugiyama, G. L. Galea, W. J. Browne, L. E. Lanyon, and J. S. Price, "Male mice housed in groups engage in frequent fighting and show a lower response to additional bone loading than females or individually housed males that do not fight," *Bone*, vol. 54, no. 1, pp. 113–7, 2013.

[22] N. Holguin, M. D. Brodt, M. E. Sanchez, A. A. Kotiya, and M. J. Silva, "Adaptation of tibial structure and strength to axial compression depends on loading history in both c57bl/6 and balb/c mice," *Calcif Tissue Int*, vol. 93, no. 3, pp. 211–21, 2013.

[23] M. E. Lynch, D. Brooks, S. Mohanan, M. J. Lee, P. Polamraju, K. Dent, L. J. Bonassar, M. C. van der Meulen, and C. Fischbach, "In vivo tibial compression decreases osteolysis and tumor formation in a human metastatic breast cancer model," *J Bone Miner Res*, vol. 28, no. 11, pp. 2357–67, 2013.

[24] C. Ciani, D. Sharma, S. B. Doty, and S. P. Fritton, "Ovariectomy enhances mechanical load-induced solute transport around osteocytes in rat cancellous bone," *Bone*, vol. 59, no. 0, pp. 229–234, 2014.

[25] J. C. Fritton, E. R. Myers, T. M. Wright, and M. C. van der Meulen, "Bone mass is preserved and cancellous architecture altered due to cyclic loading of the mouse tibia after orchidectomy," *J Bone Miner Res*, vol. 23, no. 5, pp. 663–71, 2008.

[26] M. Sinnesael, M. R. Laurent, F. Jardi, V. Dubois, L. Deboel, P. Delisser, G. J. Behets, P. C. D'Haese, G. Carmeliet, F. Claessens, and D. Vanderschueren, "Androgens inhibit the osteogenic response to mechanical loading in adult male mice," *Endocrinology*, p. en20141673, 2015.

[27] M. D. Martinez, G. J. Schmid, J. A. McKenzie, D. M. Ornitz, and M. J. Silva, "Healing of non-displaced fractures produced by fatigue loading of the mouse ulna," *Bone*, vol. 46, no. 6, pp. 1604–12, 2010.

[28] M. J. Gardner, M. C. H. v. d. Meulen, D. Demetrakopoulos, T. M. Wright, E. R. Myers, and M. P. Bostrom, "In vivo cyclic axial compression affects bone healing in the mouse tibia," *Journal of orthopaedic research : official publication of the Orthopaedic Research Society*, vol. 24, no. 8, pp. 1679–1686, 2006.

[29] J. C. Fritton, E. R. Myers, T. M. Wright, and M. C. van der Meulen, "Loading induces site-specific increases in mineral content assessed by microcomputed tomography of the mouse tibia," *Bone*, vol. 36, no. 6, pp. 1030–8, 2005.

[30] M. E. Lynch, R. P. Main, Q. Xu, T. L. Schmicker, M. B. Schaffler, T. M. Wright, and M. C. van der Meulen, "Tibial compression is anabolic in the adult mouse skeleton despite reduced responsiveness with aging," *Bone*, vol. 49, no. 3, pp. 439–46, 2011.

[31] R. L. De Souza, M. Matsuura, F. Eckstein, S. C. Rawlinson, L. E. Lanyon, and A. A. Pitsillides, "Non-invasive axial loading of mouse tibiae increases cortical bone formation and modifies trabecular organization: a new model to study cortical and cancellous compartments in a single loaded element," *Bone*, vol. 37, no. 6, pp. 810–8, 2005.

[32] T. Sugiyama, L. B. Meakin, W. J. Browne, G. L. Galea, J. S. Price, and L. E. Lanyon, "Bones' adaptive response to mechanical loading is essentially linear between the low strains associated with disuse and the high strains associated with the lamellar/woven bone transition," *J Bone Miner Res*, vol. 27, no. 8, pp. 1784–93, 2012.

[33] A. M. Weatherholt, R. K. Fuchs, and S. J. Warden, "Cortical and trabecular bone adaptation to incremental load magnitudes using the mouse tibial axial compression loading model," *Bone*, vol. 52, no. 1, pp. 372–379, 2013.

[34] J. M. Wallace, R. M. Rajachar, M. R. Allen, S. A. Bloomfield, P. G. Robey, M. F. Young, and D. H. Kohn, "Exercise-induced changes in the cortical bone of growing mice are bone- and gender-specific," *Bone*, vol. 40, no. 4, pp. 1120–1127, 2007.

[35] J. M. Wallace, K. Golcuk, M. D. Morris, and D. H. Kohn, "Inbred strain-specific effects of exercise in wild type and biglycan deficient mice," *Ann Biomed Eng*, vol. 38, no. 4, pp. 1607–17, 2010.

[36] M. Hammond and J. Wallace, "Exercise prevents -aminopropionitrile-induced morphological changes to type i collagen in murine bone.," *BoneKEy Reports*, vol. 4, 2015.

[37] J. M. Wallace, K. Golcuk, M. D. Morris, and D. H. Kohn, "Inbred strain-specific response to biglycan deficiency in the cortical bone of c57bl6/129 and c3h/he mice," *Journal of Bone and Mineral Research*, vol. 24, no. 6, pp. 1002–1012, 2009.

[38] M. L. Bouxsein, S. K. Boyd, B. A. Christiansen, R. E. Guldberg, K. J. Jepsen, and R. Muller, "Guidelines for assessment of bone microstructure in rodents using micro-computed tomography," *J Bone Miner Res*, vol. 25, no. 7, pp. 1468–86, 2010.

[39] V. Glatt, E. Canalis, L. Stadmeyer, and M. L. Bouxsein, "Age-related changes in trabecular architecture differ in female and male c57bl/6j mice," *J Bone Miner Res*, vol. 22, no. 8, pp. 1197–207, 2007.

[40] T. Sugiyama, J. S. Price, and L. E. Lanyon, "Functional adaptation to mechanical loading in both cortical and cancellous bone is controlled locally and is confined to the loaded bones," *Bone*, vol. 46, no. 2, pp. 314–321, 2010.

[41] S. Mohan, C. G. Bhat, J. E. Wergedal, and C. Kesavan, "In vivo evidence of igf-iestrogen crosstalk in mediating the cortical bone response to mechanical strain," *Bone Research*, vol. 2, 2014.

[42] F. C. Ko, C. Dragomir, D. A. Plumb, S. R. Goldring, T. M. Wright, M. B. Goldring, and M. C. van der Meulen, "In vivo cyclic compression causes cartilage degeneration and subchondral bone changes in mouse tibiae," *Arthritis Rheum*, vol. 65, no. 6, pp. 1569–78, 2013.

[43] "C57bl/6 inbred mice nhsd us," *Harlan Laboratories, Inc. USA*, 2006.

4. CONCLUSIONS AND FUTURE DIRECTIONS

While the low strain study indicated that the chosen strain level, 1750 $\mu\epsilon$, did not engender a robust bone formation response, the significant decrease in microdamage accumulation, both in terms of number and length, indicates that loading is altering the existing bone tissue in some way and protecting it against the effects of ex vivo fatigue. It is possible that if the loading experiment was continued for several weeks, instead of just two, that a quantifiable bone formation response could occur and translate to geometric, molecular, and mechanical alterations. Further considerations of frequency, waveform shape, and cycles per day and how these relate to strain rates, should be made. The frequency used in the discussed studies, 2 Hz, was chosen both based on published literature using the tibial loading model and because it is in the range of physiologic loading. Increasing the rate could increase bone formation by increasing strain rate. However, when the strain rate is increased, there may be an increased risk of joint damage. Alternatively, the frequency could remain the same and instead the shape of the waveform could be changed from haversine to triangular, thus also affecting the strain rate. Finally, number of cycles per day could be increased which would result in a longer loading period which could lead to more bone formation, but also could lead to damage accumulation in the bone. Ultimately, there is a need for a greater understanding of how all the various parameters of loading affect bone formation in rapidly growing, female, C57BL/6 mice.

While loading parameters could be adjusted to stimulate more bone formation, the multistrain study, designed based on preliminary results in the low strain study and concurrently performed, provides proof that our loading set-up and profile can successfully initiate significant bone growth. The multistrain study indicated that the two week loading period used is adequate in engendering a bone formation response if

the strain is increased to 2050 $\mu\epsilon$. These results are promising and future studies could be designed utilizing this strain level without changing other loading parameters.

In future studies, age effects should be carefully considered. A baseline group would allow for a separation of bone growth due to loading and bone growth due to aging. Additionally, because a robust formation response was not seen here, as indicated by the histomorphometric analysis, a different starting age may be considered as well. Perhaps slightly younger animals would have more bone growth over the loading period, or perhaps a slightly older animal with more mature tissue would better respond to the loading treatment. To further investigate the ability of mechanical loading to recover losses due to disease, a different disease model could be chosen. The osteogenesis imperfect (OI) disease model would provide diseased tissue at the start of loading, compared to the BAPN injections which only affect newly formed tissue. In addition, OI is more relevant to study as it affects more of the population than osteolathrysm. OI bones are extremely brittle, and it is possible that the 2050 $\mu\epsilon$ loading would cause in vivo fractures. Perhaps with an OI disease model, a longer duration of loading at lower strain levels would reduce this fracture risk.

It was an original intention of the low strain tibial loading study to use atomic force microscopy to image and quantify the mean and distribution of collagen fibril D-spacing. It was decided after initial results indicated an absence of robust bone formation response that this technique would not be used, as it is costly and time consuming. Further studies could continue this technique on bones both from this study and from future studies where mice are loaded to the mid-strain level.

In conclusion, though the expected bone response was not present in the initial low strain tibial loading study, some tissue-level changes were identified and the multistrain tibial loading study allowed for the identification of a strain level that does engender robust bone formation. The results from both of these studies, that low strain loading can induce some tissue-level changes in a two-week loading experiment and that a slightly higher strain level induces significant bone formation over the same loading period, provide promising support for the use of in vivo tibial loading

as a tool to investigate the mechanical implications of mechanical load on healthy and diseased bone.